European Journal of Medicinal Chemistry 84 (2014) 382–394

Contents lists available at ScienceDirect

European Journal of Medicinal Chemistry

journal homepage: http://www.elsevier.com/locate/ejmech

Original article

Discovery of azetidine based ene-amides as potent bacterial enoyl ACP reductase (FabI) inhibitors☆

Mohamed Takhi [a], Kandepu Sreenivas [a], Chandrashekar K. Reddy [a], Mahadari Munikumar [a], Kolakota Praveena [a], Pabolu Sudheer [a], Bandaru N.V.M. Rao [a], Gollamudi Ramakanth [a], Jampala Sivaranjani [a], Shardaprasad Mulik [a], Yeruva R. Reddy [a], Krishnamurthy Narasimha Rao [b], Rentala Pallavi [b], Anirudha Lakshminarasimhan [b], Sunil K. Panigrahi [b], Thomas Antony [b], Iskandar Abdullah [c], Yean K. Lee [c], Murali Ramachandra [b], Rohana Yusof [d], Noorsaadah A. Rahman [c], Hosahalli Subramanya [b, *]

[a] Aurigene Discovery Technologies Ltd, Bollaram Road, Miyapur, Hyderabad 500 049, India
[b] Aurigene Discovery Technologies Ltd, 39-40, KIADB Industrial Area, Phase II, Electronic City, Hosur Road, Bangalore 560 100, India
[c] Department of Chemistry, Faculty of Science, University of Malaya, 50603 Kuala Lumpur, Malaysia
[d] Department of Molecular Medicine, Faculty of Medicine, University of Malaya, 50603 Kuala Lumpur, Malaysia

ARTICLE INFO

Article history:
Received 31 January 2014
Received in revised form
9 July 2014
Accepted 10 July 2014
Available online 11 July 2014

Keywords:
FabI inhibitor
Enoyl ACP reductase
Antibacterial
Azetidine
Ene-amide

ABSTRACT

A novel and potent series of ene-amides featuring azetidines has been developed as FabI inhibitors active against drug resistant Gram-positive pathogens particularly staphylococcal organisms. Most of the compounds from the series possessed excellent biochemical inhibition of *Staphylococcus aureus* FabI enzyme and whole cell activity against clinically relevant MRSA, MSSA and MRSE organisms which are responsible for significant morbidity and mortality in community as well as hospital settings. The binding mode of one of the leads, **AEA16**, in *Escherichia coli* FabI enzyme was determined unambiguously using X-ray crystallography. The lead compounds displayed good metabolic stability in mice liver microsomes and pharmacokinetic profile in mice. The in vivo efficacy of lead **AEA16** has been demonstrated in a lethal murine systemic infection model.

1. Introduction

The emergence of bacterial resistance continues to hamper the effectiveness of existing antibacterial therapies and poses serious threat worldwide in community and nosocomial settings. Multidrug-resistant Gram-positive bacteria such as methicillin-resistant *Staphylococcus aureus* (MRSA), *Staphylococcus epidermidis* (MRSE) and vancomycin-resistant *S. aureus* (VRSA) are of major concern [1]. This challenge is further exacerbated by the reduced interest of major pharmaceutical companies in antibacterial drug discovery leading to paucity in new antibiotics pipeline [2]. Hence, there is a pressing need for increased and accelerated efforts to identify new therapeutics based on novel mechanism of action to combat bacterial resistance. In recent times, there has been a great deal of interest in targeting bacterial fatty acid biosynthesis (FAB) as a viable strategy to develop novel antibacterial agents.

The bacterial fatty acid synthase system (FASII) utilizes discrete monofunctional enzymes that operate in conjunction with acyl carrier protein (ACP)-associated substrates. In mammalian fatty acid synthase (FASI) pathway, lipid biosynthesis is mediated by a single multifunctional enzyme-ACP complex. The differences in prokaryote and eukaryote fatty acid biosynthesis provide an opportunity for selective FASII inhibition [3,4]. The inhibition of FASII pathway causes the breakdown of cell wall and disruption of cell membrane demonstrating its importance for bacterial survival [5].

FabI is an enoyl-ACP reductase that catalyses the ultimate and rate limiting step of chain elongation in each cycle in FASII pathway. The reaction involves the conjugate reduction of an enoyl-ACP to the corresponding acyl-ACP using the cofactor NADH or NADPH as a hydride source as shown in Scheme 1 [3–6]. FabI is an essential

☆ Aurigene Publication No H-05-0201-2012.
* Corresponding author.
E-mail address: hosahalli_s@aurigene.com (H. Subramanya).

http://dx.doi.org/10.1016/j.ejmech.2014.07.036
0223-5234/

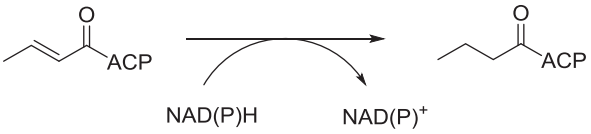

Scheme 1. FabI biosynthetic reaction.

enzyme for the viability of several bacteria and shows low degree of sequence homology with mammalian enzymes [3]. Several isoforms (FabI, FabK, FabL and FabV) of enoyl-ACP reductases (FabI isozymes) have been reported in literature [3,7,8]. Different bacteria have been reported to have one or more of these isoforms. For example, single isoform, FabI is found in *S. aureus* and *Escherichia coli*, and FabK is present in *Staphylococcus pneumoniae*. However, two isoforms FabI and FabV are present in *Pseudomonas aeruginosa* and FabI and FabL are present in *Bacillus subtilis*. These isoforms of enoyl ACP-reductases have high sequence and structural similarities. However, there are differences in the active site of these enzymes. Therefore, development of inhibitors that act on all the isoforms leading to broad spectrum activity could be challenging.

The novel mechanism of action with a potential for activity against drug resistant staphylococcal bacteria has led to the discovery of several FabI inhibitors based on different chemotypes. These include indole naphthyridinones [9], 2,34,5-tetrahydro-1H-pyrido[2,4-b and e] [1,4] diazepines [10], spiro-naphthyridinone piperidines [11], 1,2,3,4-tetrahydropyrido-indoles [12], 4-pyridones [13,14], biphenyl ethers [15] and aminopyridines [16]. Representative FabI inhibitors are shown in Fig. 1. **AFN-1252** [17], **MUT-056399** (FAB-001) [18] and **CG-400549** [19] have advanced to clinical trials for the treatment of Gram-positive bacterial infections caused by MSSA, MRSA and MRSE pathogens. Triclosan, a widely used biocide in a variety of consumer products, is known to act via FabI inhibition [20].

In pursuit of our antibacterial drug discovery programs [21,22], we were interested in developing novel and potent FabI inhibitors for the treatment of drug resistant staphylococcal infections. The efforts in this direction led to the development of a novel series of FabI inhibitors featuring azetidine ene-amides (AEAs) showing excellent in vitro and in vivo profile. This paper outlines the design, synthesis, SAR, metabolic stability, in vivo pharmacokinetic profile and in vivo antibacterial activity of a series of azetidine ene-amides (AEAs).

2. Results and discussion

2.1. Initial design of FabI inhibitors

We used structure-guided approach based on X-ray structure of **AFN-1252** bound to *E. coli* FabI determined in-house [23]. Critical interactions observed between **AFN-1252** and *E. coli* FabI are shown in Fig. 2. The pyridine nitrogen and amidic NH makes two H-bonds with residue Ala-95 while the carbonyl oxygen in the ene-amide moiety is engaged in H-bond interaction with NADH and side chain of Tyr-156 residue. The benzofuran ring occupies a hydrophobic pocket formed by the residues Tyr-146, Met-159 and Phe-203 and makes a favourable π-stacking interaction with residue Tyr-146. The methyl substitution on benzofuran moiety at 3-position further enhances this stacking interaction.

The crystal structure of **AFN-1252** bound to *E. coli* FabI revealed that ample space is available around the ene-amidic nitrogen for the design of novel FabI inhibitors. Keeping these observations in view, we designed novel FabI inhibitors by introducing azetidine ring which is capable of producing conformationally rigid amides that are relatively resistant to enzymatic hydrolysis compared to

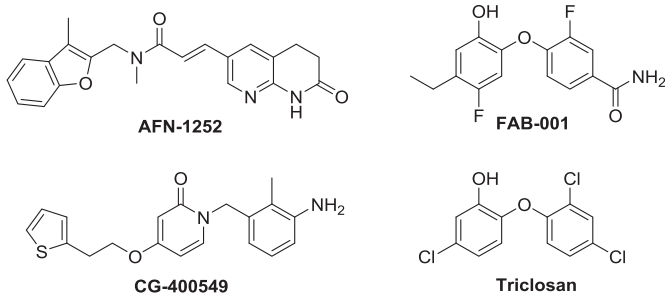

Fig. 1. FabI inhibitors.

open chain amides (Fig. 3) [24,25]. We envisaged that such modification could engender compounds with good metabolic stability and pharmacokinetic profile while retaining the potency. Indeed, the initial compounds **AEA2** and **AEA3** did show *S. aureus* FabI enzyme inhibition when tested at 1 μM concentration as shown in Fig. 3.

2.2. Design, synthesis and SAR of substituted azetidine ene amides (AEAs) with naphthyridinon-one on right hand side

Encouraged by the biochemical data of initial compounds **AEA2** and **AEA3** we set out to investigate further the effect of azetidines on SAR paradigm of ene-amide scaffold through iterative medicinal chemistry approach. We initiated our efforts by varying different substitutions on azetidine moiety on the left hand side (LHS) followed by the modification of cyclic amide ring on right hand side (RHS) as shown in Fig. 3.

The first iteration of SAR was focussed on the left hand side, exploring the hydrophobic pocket in the FabI active site. Accordingly, several analogues with structurally diverse and lipophilic substitutions at the 3-position of azetidine as exemplified by azetidine ene-amides **AEA4-21** were designed and synthesized. We hypothesized that these LHS substitutions on azetidine could optimize interactions in the hydrophobic pocket and thereby enhance biochemical and in vitro antibacterial activity.

The synthesis of azetidine ene-amides **AEA1-12** is delineated in Scheme 2. The key carboxylic acid intermediate **1** has been conveniently prepared according to the literature procedure [9]. The compound **AEA1** [25] was made by coupling acid **1** and

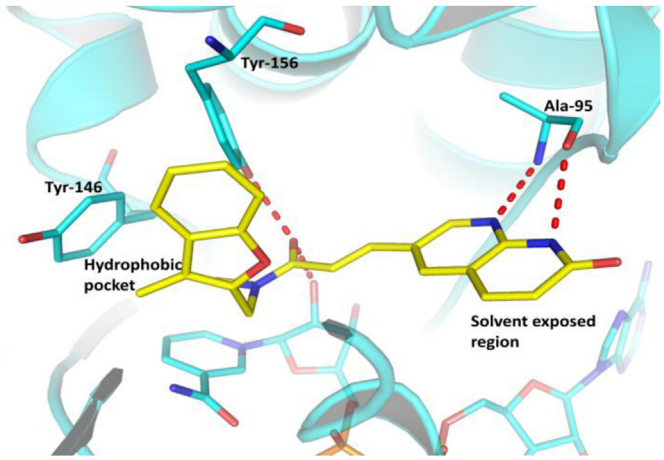

Fig. 2. X-ray structure of **AFN-1252** (shown in yellow) in complex with *E. coli* FabI. NADH is shown in cyan colour. Hydrogen bond interactions are shown in dotted lines.

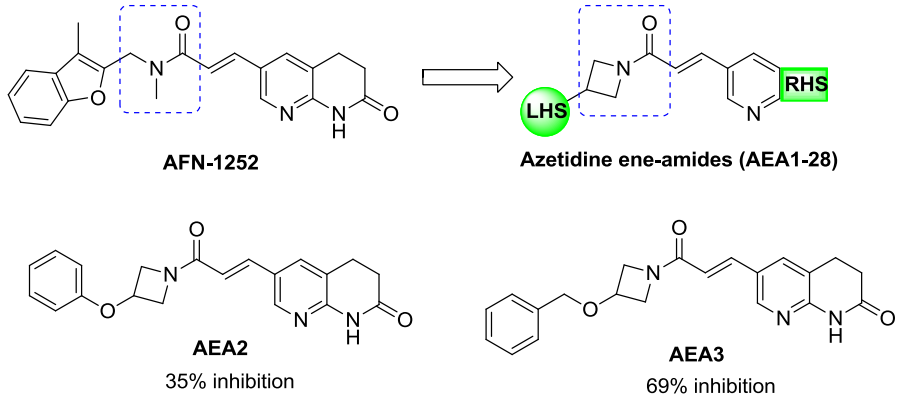

Fig. 3. Design of azetidine ene-amide series and initial hits.

commercially available azetidine **2** under **EDC·HCl** and **HOBt** conditions in the presence of Hunig's base. The substituted azetidine counterparts have been accessed by different routes following reported procedures and coupled with the carboxylic acid **1** to produce final molecules. Compounds **AEA2** and **AEA3** have been made starting from readily available amines **3** and **4** respectively [25]. The azetidine amides **AEA4-11** were obtained by coupling acid **1** and the amines **5**–**12** made following literature procedures [26]. The base promoted *O*-arylation of alcohol **13** with 2-chloro benzothiazole in the presence of sodium hydride furnished **14** which in turn was treated with trifluoroacetic acid followed by coupling with acid **1** to yield **AEA12**.

The synthesis of carbon linked azetidines (**AEA13**–**21**) was executed as represented in Scheme 3. Benzothiazole nucleus was introduced to the azetdine **15** [27] employing the Minisci reaction conditions [28]. The radical mediated oxidative coupling of benzothiazole and **15** in the presence of hydrogen peroxide and ferrous sulphate produced the azetidine derivative **16** which subsequently furnished **AEA13**. Similarly, azetidine intermediates **18**–**24** were synthesized by reacting iodide **17** [28] with corresponding heteroaryls under the Minisci reaction conditions. The transformation of these intermediates to final compounds **AEA14**–**20** followed routine procedures. The compound **AEA21** was smoothly obtained by coupling commercially available phenyl-3-azetidine with acid **1** under standard amide coupling conditions.

The final compounds were screened in a *S. aureus* FabI biochemical assay followed by whole cell assay comprising a panel of MSSA, MRSA and MRSE organisms. As shown in Table 1, introduction of azetidine resulted in potent FabI inhibitors illustrating a range of tolerable substitutions on azetidine ring.

Unsubstituted analogue **AEA1** is inactive probably because of the lack of a group occupying the hydrophobic pocket. However, substituted azetidines that have moieties interacting with hydrophobic pocket demonstrated good biochemical and cell based activities. Among the azetidinyl ethers **AEA3** and **AEA4**, a noticeable increase in FabI potency and whole cell activity was observed when oxygen is in conjugation with phenyl moiety with a methylene spacer as exemplified by **AEA4** (IC_{50} = 0.265 μM, MIC = 0.25–1 μg/mL). The fluoro phenyl derivatives **AEA5-7**, in general, showed good FabI enzyme activity and the p-fluoro phenyl analogue **AEA7** showed superior antibacterial activity with MICs in the range of 0.25–1 μg/mL compared to other fluoro phenyl analogues. In the case of methyl substituted phenyl analogues **AEA8-10**, ortho derivative **AEA8** possessed potent enzyme activity (IC_{50} = 0.177 μM) which translated into good whole cell activity (MIC = 0.25–1 μg/mL) compared to other isomers. Introduction of biaryl moieties on azetidine through oxymethylene (**AEA11**), oxygen (**AEA12**) and methylene (**AEA13**) spacers yielded compounds with poor to moderate potency which could be due to unfavourable geometry leading to the loss of π-stacking interaction with Tyr-146. In contrast, direct linkage of biaryl moiety to azetidine exemplified by **AEA14** led to dramatic improvement in FabI inhibition (IC_{50} = 0.373 μM) as well as cell based activity against staphylococcal strains (MIC = 0.25–1 μg/mL). Encouraged by this SAR finding, a few more analogues (**AEA15**–**21**) were made wherein an aryl or a biaryl moiety is directly attached to azetidine at the 3-position through carbon–carbon linkage as mentioned in Scheme 3.

In a gratifying result, installation of 3-methyl benzoxazole on azetidine afforded the compound **AEA16** with improved FabI enzyme inhibition (IC_{50} = 0.141 μM) and the best antibacterial activity against various staphylococcal organisms (MIC = 0.06–0.5 μg/mL). The 5-methoxy-benzoxazole **AEA17** and 5-chloro benzoxazole

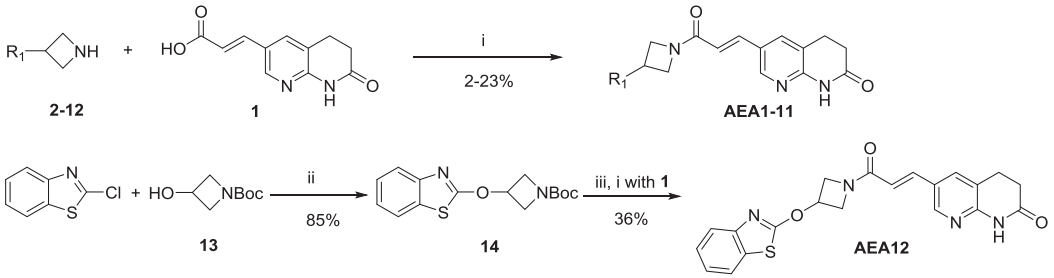

Scheme 2. Reagents and conditions: (i) **EDC·HCl**, **HOBt**, DIPEA, r.t, overnight; (ii) NaH, DMF, 100 °C, overnight; (iii) TFA, CH_2Cl_2, r.t, 2 h. R_1 = H, **2**, **AEA1**; R_1 = PhO, **3**, **AEA2**; R_1 = $PhCH_2O$, **4**, **AEA3**; R_1 = $PhOCH_2$, **5**, **AEA4**; R_1 = o-fluoro-C_6H_4-OCH_2, **6**, **AEA5**; R_1 = m-fluoro-C_6H_4-OCH_2, **7**, **AEA6**; R_1 = p-fluoro-C_6H_4-OCH_2, **8**, **AEA7**; R_1 = o-methyl-C_6H_4-OCH_2, **9**, **AEA8**; R_1 = m-methyl-C_6H_4-OCH_2, **10**, **AEA9**; R_1 = p-methyl-C_6H_4-OCH_2, **11**, **AEA10**; R_1 = 2-napthyl-OCH_2, **12**, **AEA11**.

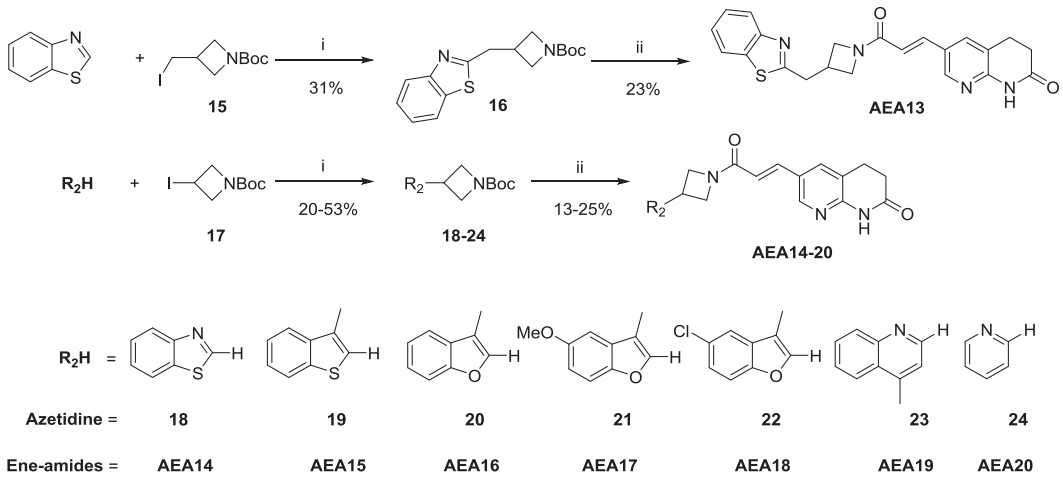

Scheme 3. Reagents and conditions: (i) $FeSO_4 \cdot 7H_2O$, H_2SO_4, H_2O_2, DMSO, r.t, 16 h; (ii) (a) TFA, CH_2Cl_2, r.t, 2 h (b) 1, EDC·HCl, HOBt, DIPEA, r.t, overnight.

AEA18 exhibited good in vitro antibacterial profile. However, quinoline **AEA19** and pyridine **AEA20** exhibited poor to moderate whole cell activity, presumably due to poor cell permeability of molecule and/or efflux barriers present in bacterial membrane.

2.3. Design, synthesis and SAR of benzofuranyl-azetidine ene amides with variation on right hand side

Having established SAR on left hand side, we turned our attention to the right hand side (RHS) part of the ene-amide scaffold. In this iteration, modifications were carried out on the potent compound **AEA16** keeping the 2-benzfuranyl azetidine moiety constant. Substitutions on RHS occupy a hydrophilic pocket and compounds with basic functionalities in this region have been previously reported [10,11]. Accordingly, a cross section of analogues with variations (**AEA22**–**28**) on pyridine ring have been made and screened.

Compounds**AEA22**–**24** have been prepared by coupling amine **25**, obtained from **20**, with corresponding acids **26** [9], **27** [29] and **28** [30] as shown in Scheme 4. The azetidine ene-amides **AEA25**–**28** were synthesized in a convergent manner as delineated in Scheme 5. The bromo-diazepinone intermediates **30** [10], **31** [10], **32** [31], **33** [10] have been obtained according to literature procedures and coupled to acrylamide **29** under Heck reaction conditions to furnish corresponding products **AEA25**–**28**.

These analogues were also tested in biochemical and whole cell assays. The results are summarized in Table 2. Although its enzyme activity is retained, the acetamide **AEA22** showed inferior cell based activity compared to its cyclic congener **AEA16**. Surprisingly, 1,2,3-triazole substituted acetamide **AEA23** showed poor biochemical and antibacterial activities which could be due to the disturbance in a hydrogen bonding network between the backbone carbonyl and amide hydrogen of Ala-95 from *S. aureus* FabI enzyme. The substitution of N-alkyl morpholine onto cyclic urea yielded highly potent FabI inhibitor **AEA24** with IC_{50} of 58 nM. This observation is reminiscent to the results reported by the Affinium group wherein the basic appendage can occupy the solvent pocket away from the target site [11]. The N-methyl diazepinone **AEA26** was found to be equipotent to its corresponding N–H diazepinone **AEA25** and showed MICs in the range of 0.25–0.5 μg/mL. Extended substitutions on diazepinone yielded less potent **AEA27** compared to **AEA24** which could be due to inability of this morpholine group to access the solvent pocket. The compound **AEA28** showed almost equal biochemical potency and cell based activity to its positional isomer **AEA25**.

Above SAR results indicate that right combination of groups on both sides of ene-amide scaffold is essential for achieving good FabI potency as well as in vitro antibacterial activity. Further, in addition to biochemical potency, appropriate balance of physicochemical properties such as clogP, molecular weight and polarity are critical to overcome bacterial cell membrane permeability barriers [32]. Therefore, the variation in MIC values of these compounds can be a consequence of differences in their aforementioned properties. Among these compounds, best in vitro antibacterial activity (MIC = 0.06 μg/mL) is obtained against MRSA and MSSA organisms for **AEA16** which possess a naphthyridinone ring on the right hand side and benzofuranyl moiety on left hand side. These structural features are similar to **AFN-1252** as shown in Fig. 4.

An X-ray crystal structure of one of the leads **AEA16** bound to *E. coli* FabI enzyme (Fig. 5) in the presence of NADH was determined to a resolution of 3.2 Å [33] and it was found to be similar to other crystal structures reported from the ene-amide series [9].

A superposition of **AEA16**, **AFN-1252** and triclosan X-ray structures (PDB ID: 1C14) is shown in Fig. 6. It is evident that critical interactions observed in **AFN-1252** are conserved in **AEA16** bound *E. coli* FabI complex. Benzofuran moieties in the **AEA16** and **AFN-1252**, and chlorine atom in triclosan occupy the same hydrophobic pocket. Hydroxyl moiety of triclosan is hydrogen bonded to Tyr-156 and NADH whereas oxygen atoms of carbonyls of **AFN-1252** and **AEA16** in the ene-amide moiety are engaged in hydrogen boding with the same residues. This key hydrogen bond interaction with Tyr-156 residue is also reported in several known FabI inhibitors [9,17,34,35].

2.4. Metabolic stability and in vivo pharmacokinetic profile of selected compounds

Selected compounds possessing good cell based activity were tested for metabolic stability in mice liver microsomes. The compounds showing good metabolic stability were further evaluated for in vivo pharmacokinetic properties in mice by oral route. The results are summarized in Table 3. Most of these azetidine ene-amides, except **AEA26**, were found to have high metabolic stability. The good metabolic stability of these analogues could be due to enzymatic stability of cyclic and conformationally restricted azetidine amide. The compound **AEA26** appears to be metabolically less stable likely because of demethylation of diazepinone ring by liver enzymes [36]. **AFN-1252** was found to be less stable compared to azetidine ene-amide analogues presumably due to the presence of open chain amide as discussed. Most of these compounds

Table 1
SAR on LHS part of ene-amide.

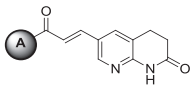

Compound no	A	*S. aureus* FabI inhibition		MIC (μg/mL)[a]		
		%@1 μM	IC_{50}(μM)	MSSA[b]	MRSA[c]	MRSE[d]
AEA1		15%	ND[e]	>32	>32	>32
AEA2	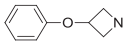	35%	ND[e]	4	4	16
AEA3	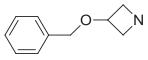	69%	0.376	1	2	2
AEA4	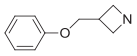	81%	0.265	0.25	0.25	1
AEA5	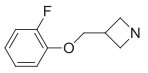	99%	0.378	1	1	2
AEA6	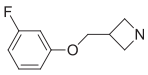	89%	0.438	1	2	2
AEA7	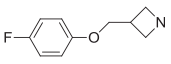	92%	0.316	0.25	0.5	1
AEA8	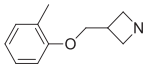	80%	0.177	0.25	0.5	1
AEA9	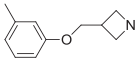	47%	ND	2	2	2
AEA10	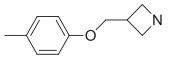	67%	0.921	1	1	2
AEA11	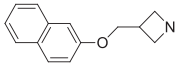	68%	1.41	4	4	>32
AEA12	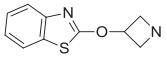	16%	ND[e]	>32	>32	>32
AEA13	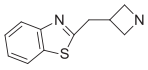	41%	ND[e]	2	4	2
AEA14	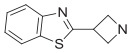	83%	0.373	0.25	0.25	1
AEA15	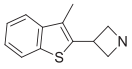	89%	0.709	0.125	0.25	2
AEA16	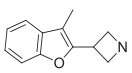	96%	0.141	0.06	0.06	0.5
AEA17	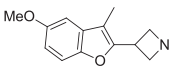	ND[e]	ND[e]	0.5	1	2
AEA18	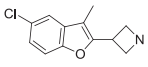	82%	0.204	0.25	0.25	0.5
AEA19	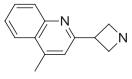	84%	0.242	32	>32	>32

Table 1 (*continued*)

Compound no	A	*S. aureus* FabI inhibition		MIC (μg/mL)[a]		
		%@1 μM	IC_{50}(μM)	MSSA[b]	MRSA[c]	MRSE[d]
AEA20	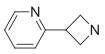	87%	0.242	4	8	16
AEA21	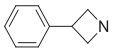	80%	0.488	1	2	2

[a] MIC = Minimum inhibitory concentration.
[b] MSSA – methicillin-sensitive *Staphylococcus aureus* ATCC 29213.
[c] MRSA – methicillin-resistant *Staphylococcus aureus* ATCC 33591.
[d] MRSE – methicillin-resistant *Staphylococcus epidermidis* AUCC 704.
[e] ND = Not determined.

possessed excellent pharmacokinetic profile with good systemic exposures as exemplified by **AEA7**, **AEA14**, **AEA16** and **AEA18.** Among these compounds **AEA8**, **AEA15** and **AEA25** showed relatively lower AUC and C_{max} values compared to the rest of the molecules. Higher rate of clearance due to lower metabolic stability of **AEA8** and **AEA15** could be contributing to lower AUC and C_{max} values compared to other compounds. Despite the good metabolic stability, **AEA25** showed suboptimal pharmacokinetics which could be a consequence of poor absorption. **AFN-1252** displayed a poor pharmacokinetic profile compared to these azetidine-ene amides presumably due to its poor metabolic stability in mice liver microsomes.

2.5. *In vivo efficacy of compound **AEA16***

Based on potent cell based activity (MIC = 0.06 μg/mL) and favourable pharmacokinetic profile, compound **AEA16** was advanced to in vivo efficacy studies in a lethal murine systemic infection model by oral route, employing MRSA as the infectious organism. The results are presented in Table 4. **AEA16** protected the mice from infection at the ED_{50} dose of 0.90 mg/kg/day which was superior to that of Linezolid (ED_{50} = 2.8 mg/kg/day), a current standard of care for the treatment of MRSA infections. The potent in vitro antibacterial activity of lead **AEA16** coupled with good pharmacokinetic profile led to impressive in vivo efficacy.

3. Conclusions

In summary, we have developed a potent and promising series of ene-amides bearing azetidines as FabI inhibitors active against a panel of resistant staphylococcal organisms. Structure-guided SAR in iterative approach through the introduction of structurally diverse azetidines followed by right hand side modifications afforded potent compounds with excellent FabI inhibition ($IC_{50} \geq 0.058$ μM) and antibacterial activity (MICs ≥0.06 μg/mL) against MSSA, MRSA and MRSE pathogens. Excellent metabolic stability and pharmacokinetic properties have been observed for the compounds from this series. The lead **AEA16** demonstrated very good in vivo efficacy in a murine systemic infection model. The key SAR insights in this program will be utilized for further optimization of ene-amide series to identify a clinical candidate.

4. Experimental

4.1. General

All chemicals were purchased from Sigma–Aldrich, Lancaster and Combiblock and were used without further purification. Reactions were monitored by TLC performed on silica gel aluminium

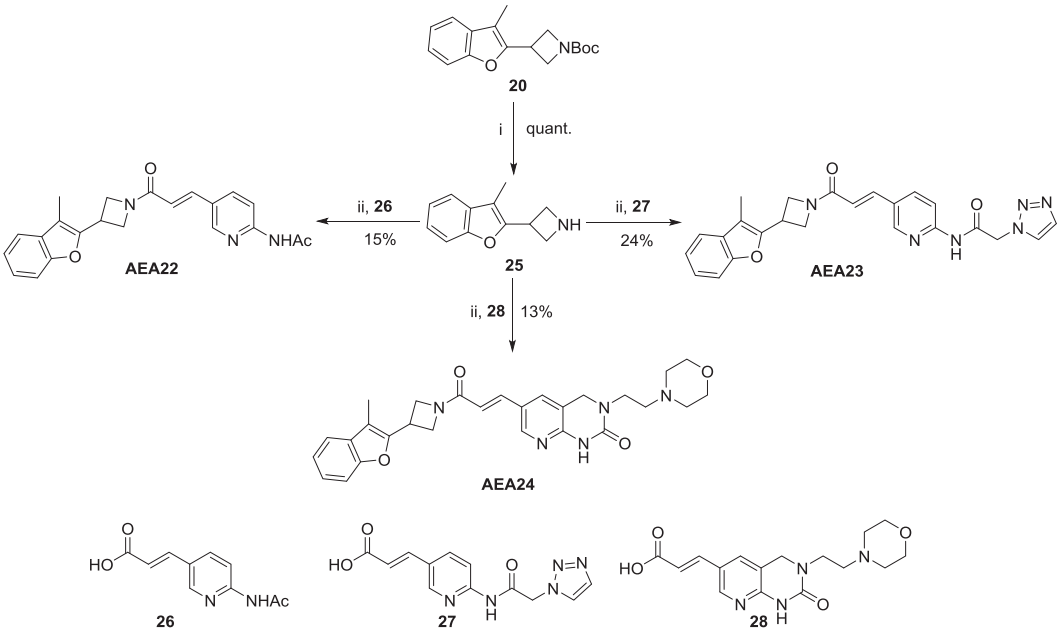

Scheme 4. Reagents and conditions: (i) TFA, CH_2Cl_2, r.t, 2 h; (ii) EDC·HCl, HOBt, DIPEA, r.t, overnight.

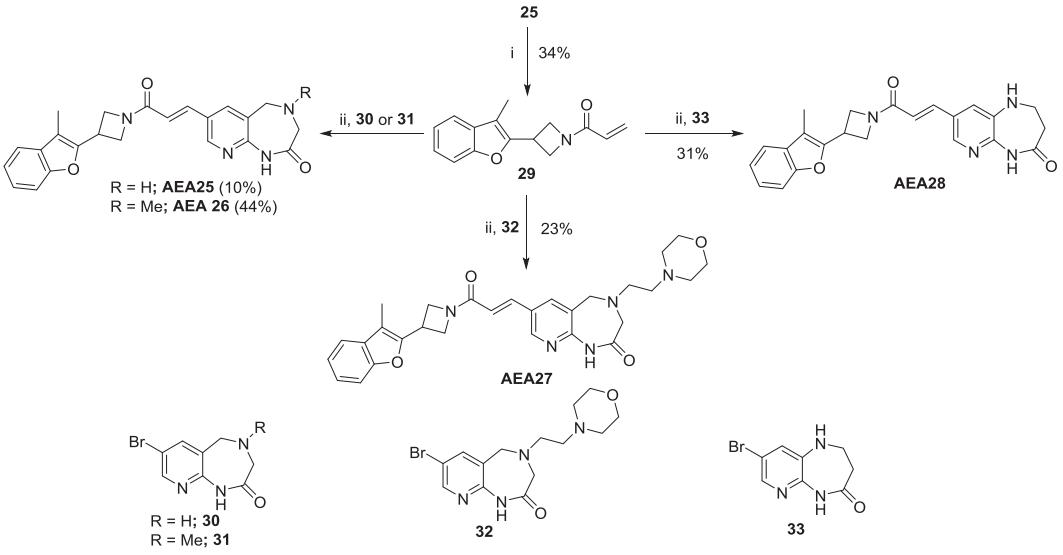

Scheme 5. Reagents and conditions: (i) Acryloyl chloride, Et_3N, CH_2Cl_2, r.t, 16 h; (ii) $Pd(OAc)_2$, P(o-tolyl)$_3$, DIPEA, Propionitrile, reflux, 6 h.

plates containing 60 F254. Column chromatography was performed with Merck 100–200 mesh silica gel. ^{1}H NMR and ^{13}C NMR were recorded on Varian Mercury Plus (400 MHz) or Varian Unity Inova (500 MHz) instruments. Chemical shifts are reported in parts per million (δ in ppm) relative to the peak for tetramethylsilane (TMS) as internal standard and the coupling constants are reported in Hertz (Hz). High resolution mass spectra (HRMS) were recorded on a Waters LCT-Premier mass spectrometer. IR spectra were recorded on a FT-IR spectrometer and only major peaks are reported in cm^{-1}.

4.2. General procedure for the synthesis of ***AEA1-24***

Diisopropyl ethyl amine (3 equiv) was added to a stirred solution of **azetidine or substituted** azetidine-TFA salt (1.1 equiv), carboxylic acid **1** (1 equiv), **HOBt** (2 equiv) and **EDC·HCl** (2 equiv) in DMF (10 volumes) at room temperature. The reaction mixture was stirred at the same temperature for 16 h, then diluted with H_2O (50 volumes) and extracted with ethyl acetate (3 × 50 volumes). The combined organic layers were washed with brine (50 volumes), dried over Na_2SO_4, filtered and volatiles were removed under vacuum. The crude residue was purified by column chromatography to furnish the desired products **AEA1-24**.

4.2.1. *(E)-6-(3-(azetidin-1-yl)-3-oxoprop-1-en-1-yl)-3,4-dihydro-1,8-naphthyridin-2(1H)-one (**AEA1**)*

Yield: 9%; White solid; mp: 278–279 °C; IR (KBr, cm^{-1}): 3535, 2883, 1654, 1598, 1462, 1300, 1197, 983, 852, 530; ^{1}H NMR (400 MHz, DMSO-d_6): δ_H 10.64 (s, 1H), 8.33 (d, J = 1.5 Hz, 1H), 8.00 (s, 1H), 7.38 (d, J = 15.9 Hz, 1H), 6.69 (d, J = 15.9 Hz, 1H) 4.28 (t, J = 7.6 Hz, 2H), 3.94 (t, J = 7.6 Hz, 2H), 2.91 (t, J = 7.6 Hz, 2H), 2.58–2.52 (m, 2H), 2.28–2.20 (m, 2H); ^{13}C NMR (500 MHz, DMSO-d_6): δ_C 14.8, 23.2, 30.0, 47.6, 49.8, 116.1, 119.0, 125.3, 133.5, 136.3,

Table 2
SAR on RHS part of ene-amide.

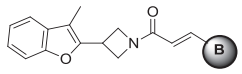

Compound no	B	*S. aureus* FabI inhibition		MIC μg/mL[a]		
		%@1 μM	IC_{50}(μM)	MSSA[b]	MRSA[c]	MRSE[d]
AEA22	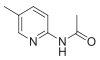	97%	0.161	1	1	8
AEA23	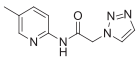	66%	0.843	>32	>32	>32
AEA24	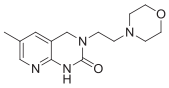	105%	0.058	1	1	2
AEA25	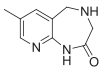	83%	0.384	0.25	0.25	1
AEA26	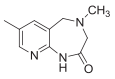	99%	0.112	0.25	0.25	0.5
AEA27	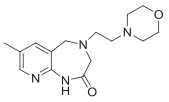	100%	0.289	1	1	2
AEA28	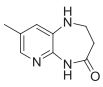	92%	0.316	0.25	0.5	1
AFN-1252		100%	0.029	0.008	0.008	0.008

[a] MIC = Minimum inhibitory concentration.
[b] MSSA – methicillin-sensitive *Staphylococcus aureus* ATCC 29213.
[c] MRSA- methicillin-resistant *Staphylococcus aureus* ATCC 33591.
[d] MRSE – methicillin-resistant *Staphylococcus epidermidis* AUCC 704.

147.1, 152.3, 164.8, 170.9; HRMS *m/z* Calcd for $C_{14}H_{15}N_3O_2$ $[M+H]^+$: 258.1243, Found: 258.1246.

*4.2.2. (E)-6-(3-oxo-3-(3-phenoxyazetidin-1-yl)prop-1-en-1-yl)-3,4-dihydro-1,8-naphthyridin-2(1H)-one (**AEA2**)*

Yield = 17%; White solid; mp: 244–245 °C; IR (KBr, cm^{-1}): 3061, 2873, 1658, 1600, 1489, 1354, 1236, 1192, 1024, 842, 754, 692; ^1H NMR (400 MHz, DMSO-d_6): δ_H 10.65 (brs, 1H), 8.35 (d, J = 1.9 Hz, 1H), 8.02 (s, 1H), 7.42 (d, J = 15.6 Hz, 1H), 7.35–7.31 (m, 2H), 7.00 (t, J = 7.3 Hz, 1H), 6.88 (d, J = 7.8 Hz, 2H), 6.76 (d, J = 15.6 Hz, 1H), 5.11–5.08 (m, 1H), 4.77–4.73 (m, 1H), 4.42 (dd, J = 7.0 Hz, 10.5 Hz, 1H), 4.22 (dd, J = 3.1 Hz, 9.5 Hz, 1H), 3.90 (dd, J = 3.1 Hz, 10.9 Hz, 1H), 2.90 (t, J = 7.8 Hz, 2H), 2.53 (d, J = 7.8 Hz, 2H); ^{13}C NMR (400 MHz, DMSO-d_6): δ_C 23.3, 29.9, 54.6, 57.0, 65.3, 114.6, 116.2, 119.0, 121.3, 125.2, 129.7, 133.6, 136.9, 141.2, 152.4, 156.2, 165.1, 170.9; HRMS *m/z* Calcd for $C_{20}H_{19}N_3O_3$ $[M+H]^+$: 350.1505, Found: 350.1489.

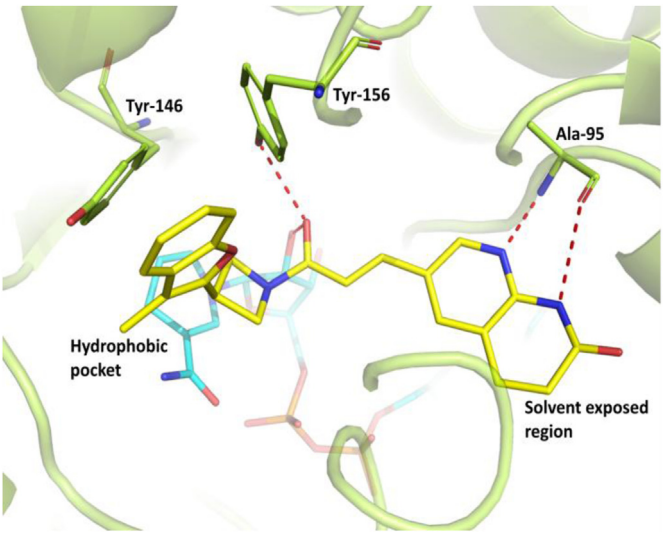

Fig. 5. X-ray structure of **AEA16** (shown in yellow) in complex with *E. coli* FabI. NADH is shown in cyan colour. Hydrogen bonded interaction is shown in dotted line.

*4.2.3. (E)-6-(3-(3-(benzyloxy)azetidin-1-yl)-3-oxoprop-1-en-1-yl)-3,4-dihydro-1,8-naphthyridin-2(1H)-one (**AEA3**)*

Yield = 22%; Off-white solid; mp: 205–206 °C; IR (KBr, cm^{-1}): 3485, 2924, 1687, 1591, 1452, 1357, 1296, 1192, 974, 846, 698, 530; ^1H NMR (400 MHz, DMSO-d_6) δ_H 10.65 (brs, 1H), 8.30 (s, 1H), 8.00 (s, 1H), 7.39 (d, J = 15.2 Hz, 1H), 7.37–7.31 (m, 5H), 6.70 (d, J = 15.6 Hz, 1H), 4.47–4.44 (m, 4H), 4.14–4.10 (m, 2H), 3.73 (d, J = 7.8 Hz, 1H), 2.91 (t, J = 7.6 Hz, 2H), 2.58–2.52 (m, 2H); ^{13}C NMR (400 MHz, DMSO-d_6): δ_C 23.3, 30.0, 54.9, 57.0, 66.9, 70.0, 116.3, 119.0, 125.2, 127.7, 127.9, 128.3, 133.5, 136.6, 137.5, 147.2, 152.4, 165.1, 170.9; HRMS *m/z* Calcd for $C_{21}H_{21}N_3O_3$ $[M+H]^+$: 364.1661, Found: 364.1666.

*4.2.4. (E)-6-(3-oxo-3-(3-(phenoxymethyl)azetidin-1-yl)prop-1-en-1-yl)-3,4-dihydro-1,8-naphthyridin-2(1H)-one (**AEA4**)*

Yield = 17%; Pale yellow solid; mp: 207–208 °C; IR (KBr, cm^{-1}): 3199, 2875, 1701, 1492, 1236, 989, 761, 528^1H NMR (400 MHz, DMSO-d_6): δ_H 8.58 (brs, 1H), 8.33 (d, J = 1.5 Hz, 1H), 7.64 (s, 1H), 7.60 (d, J = 15.6 Hz, 1H), 7.31 (d, J = 7.6 Hz, 1H), 7.29 (d, J = 7.3 Hz, 1H), 6.98 (t, J = 7.3 Hz, 1H), 6.91 (d, J = 8.0 Hz, 2H), 6.45 (d, J = 15.6 Hz, 1H), 4.45 (t, J = 8.4 Hz, 1H), 4.26 (dd, J = 8.6 Hz, 17.3 Hz, 1H), 4.23–4.18 (m, 1H), 4.17–4.12 (m, 2H), 4.10–3.99 (m, 1H), 3.64 (t, J = 6.1 Hz, 1H), 2.99 (t, J = 7.3 Hz, 2H), 2.69 (t, J = 7.3 Hz, 2H); ^{13}C NMR (500 MHz, DMSO-d_6): δ_C 23.3, 27.6, 30.0, 49.9, 52.5, 69.0, 114.5, 116.2, 119.0, 120.7, 125.3, 129.4, 133.5, 136.4, 147.1, 152.3, 158.3, 165.1, 170.9; HRMS *m/z* Calcd for $C_{21}H_{21}N_3O_3$ $[M+H]^+$: 364.1661, Found: 364.1660.

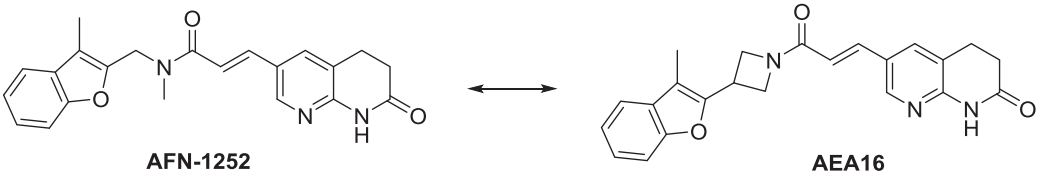

Fig. 4. Structural similarities between **AFN-1252** and **AEA16**.

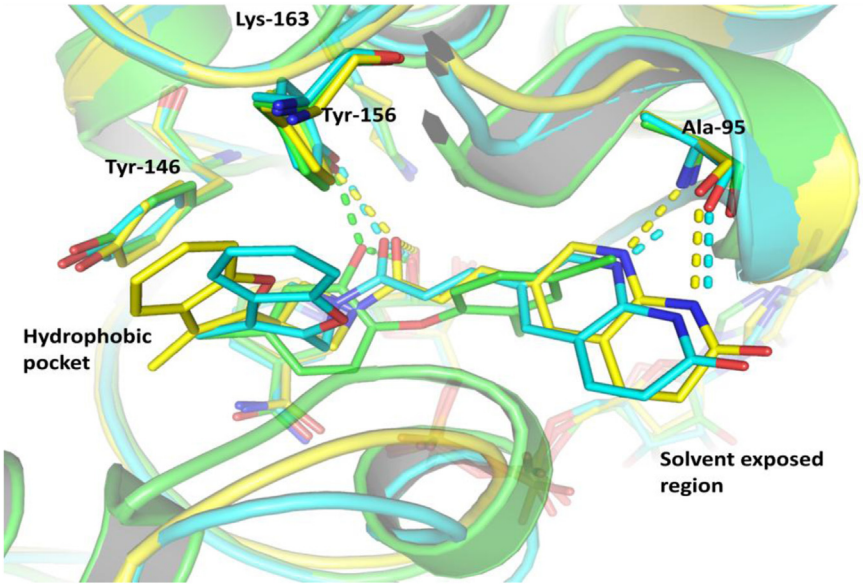

Fig. 6. Superposition of X-ray structure of **AEA16** (yellow), **AFN-1252** (cyan) and triclosan (green) in complex with *E. coli* FabI. Hydrogen bonding interaction is shown in dotted line.

Table 3
Metabolic stability and in vivo pharmacokinetic parameters of selected compounds.

Compound	Metabolic stability[a]		In vivo pharmacokinetics[b]			
	15 min	60 min	AUC (μg/mL*h)	C_{max} (μg/mL)	$t_{1/2}$ (h)	T_{max} (h)
AEA7	91.7%	83.4%	95.2	15.1	3.23	2.0
AEA8	82.1%	44.4%	38.5	7.60	4.74	2.0
AEA14	84.0%	59.9%	75.9	14.4	2.17	2.0
AEA15	65.5%	36.1%	35.5	2.79	4.11	4.0
AEA16	79.4%	55.7%	63.5	8.95	3.20	2.0
AEA18	81.0%	80.2%	86.8	8.10	2.00	1.0
AEA25	96.2%	76.4%	9.0	2.25	8.5	0.5
AEA26	25.6%	6.6%	ND[c]	ND[c]	ND[c]	ND[c]
AFN-1252	55.4%	17.5%	2.20	0.44	1.84	1.00

[a] Metabolic stability study was carried in the presence of mice liver microsomes and measured percentage of compound remaining after 15 min and 60 min.
[b] Pharmacokinetic experiments were performed in mice using single dose (10 mg/kg) through oral route of administration.
[c] ND = not determined.

*4.2.5. (E)-6-(3-(3-((2-fluorophenoxy)methyl)azetidin-1-yl)-3-oxoprop-1-en-1-yl)-3,4-dihydro-1,8-naphthyridin-2(1H)-one (**AEA5**)*

Yield = 13%; Pale yellow solid; mp: 186–187 °C; IR (KBr, cm^{-1}): 3041, 1649, 1589, 1504, 1282, 1193, 1109,842, 748; ^{1}H NMR (400 MHz, DMSO-d_6): δ_H 10.65 (s, 1H), 8.34 (s, 1H), 8.03 (s, 1H), 7.40 (d, J = 15.7 Hz, 1H), 7.22–7.12 (m, 3H), 6.98–6.94 (m, 1H), 6.74 (d, J = 15.6 Hz, 1H), 4.43 (t, J = 8.8 Hz, 1H), 4.26–4.06 (m, 4H), 3.82–3.76 (m, 1H), 3.16–3.06 (m, 1H), 2.92–2.88 (m, 2H), 2.55–2.53 (m, 2H); ^{13}C NMR (500 MHz, DMSO-d_6): δ_C 23.2, 27.6, 30.0, 49.8, 52.4, 70.3, 115.4, 116.0, 116.2, 119.0, 121.3, 124.8, 125.3, 133.5, 136.5, 146.3, 147.1, 150.8, 152.3, 165.1, 170.9; HRMS *m/z* Calcd for $C_{21}H_{20}FN_3O_3$ $[M+H]^+$: 382.1567, Found: 382.1569.

Table 4
In vivo efficacy of **AEA16** in murine systemic infection model.

Compound	ED_{50} (mg/kg)
AEA16	0.90 (0.5–1.9)[a]
Linezolid	2.30 (1.2–4.6)[a]

[a] Values in brackets denote confidence range.

*4.2.6. (E)-6-(3-(3-((3-fluorophenoxy)methyl)azetidin-1-yl)-3-oxoprop-1-en-1-yl)-3,4-dihydro-1,8-naphthyridin-2(1H)-one (**AEA6**)*

Yield = 22%; Cream colour solid; mp: 228–229 °C; IR (KBr, cm^{-1}): 2877, 1591, 1489, 1136, 950, 842,528; ^{1}H NMR (400 MHz, DMSO-d_6): δ_H 10.65 (s, 1H), 8.34 (d, J = 1.5 Hz, 1H), 8.03 (s, 1H), 7.40 (d, J = 15.7 Hz, 1H), 7.32 (q, J = 8.3 Hz, 1H), 6.87–6.78 (m, 3H), 6.74 (d, J = 15.6 Hz, 1H), 4.43 (t, J = 8.8 Hz, 1H), 4.20–4.06 (m, 4H), 3.78–3.74 (m, 1H), 3.12–3.06 (m, 1H), 2.91 (t, J = 7.8 Hz, 2H), 2.55–2.51 (m, 2H); ^{13}C NMR (500 MHz, DMSO-d_6): δ_C 23.3, 27.5, 30.0, 49.9, 52.4, 69.5, 102.0, 107.4, 110.9, 116.2, 119.0, 125.2, 130.6, 130.7, 133.5, 136.5, 147.1, 152.3, 159.9, 165.1, 170.9; HRMS *m/z* Calcd for $C_{21}H_{20}FN_3O_3$ $[M+H]^+$: 382.1567, Found: 382.1602.

*4.2.7. (E)-6-(3-(3-((4-fluorophenoxy)methyl)azetidin-1-yl)-3-oxoprop-1-en-1-yl)-3,4-dihydro-1,8-naphthyridin-2(1H)-one (**AEA7**)*

Yield = 21%; White solid; mp: 98–99 °C; IR (KBr, cm^{-1}): 2879, 1687, 1604, 1506, 1203, 829, 750; ^{1}H NMR (400 MHz, DMSO-d_6): δ_H 8.55 (brs, 1H), 8.34 (d, J = 1.9 Hz, 1H), 7.64 (d, J = 1.6 Hz, 1H), 7.58 (d, J = 15.6 Hz, 1H), 7.01–6.97 (m, 2H), 6.87–6.84 (m, 2H), 6.45 (d, J = 15.6 Hz, 1H), 4.47–4.43 (m, 1H), 4.27–4.20 (m, 2H), 4.19–4.10 (m, 2H), 4.08–3.98 (m, 1H), 3.14–3.11 (m, 1H), 2.99 (t, J = 7.6 Hz, 2H), 2.72–2.68 (m, 2H); ^{13}C NMR (400 MHz, DMSO-d_6): δ_C 23.3, 27.6, 30.0, 49.9, 52.4, 69.7, 115.7, 115.8, 115.8, 115.9, 116.2, 119.0, 125.3, 133.5, 136.4, 147.1, 152.3, 154.8, 157.7, 165.0, 170.9; HRMS *m/z* Calcd for $C_{21}H_{20}FN_3O_3$ $[M+H]^+$: 382.1567, Found: 382.1581.

*4.2.8. (E)-6-(3-oxo-3-(3-((o-tolyloxy)methyl)azetidin-1-yl)prop-1-en-1-yl)-3,4-dihydro-1,8-naphthyridin-2(1H)-one (**AEA8**)*

Yield = 27%; Yellow solid; mp: 220–221 °C; IR (KBr, cm^{-1}): 2877, 1654, 1591, 1494, 1365, 1246, 1192, 989, 750, 528; ^{1}H NMR (400 MHz, DMSO-d_6): δ_H 10.64 (brs, 1H), 8.34 (s, 1H), 8.03 (s, 1H), 7.40 (d, J = 15.7 Hz, 1H), 7.15–7.12 (m, 2H), 6.96 (d, J = 8.3 Hz, 2H), 6.85 (d, J = 7.3 Hz, 1H), 6.75 (d, J = 15.7 Hz, 1H), 4.44–4.40 (m, 1H), 4.22–4.12 (m, 2H), 4.10–4.06 (m, 1H), 3.88–3.83 (m, 1H), 3.14–3.04 (m, 1H), 2.90 (t, J = 7.8 Hz, 2H), 2.54–2.52 (m, 2H), 2.13 (s, 3H); ^{13}C NMR (500 MHz, DMSO-d_6): δ_C 15.7, 23.2, 27.8, 30.0, 49.8, 52.3, 68.7, 111.5, 116.2, 119.0, 120.4, 125.3, 125.7, 126.9, 130.3, 133.5, 136.4, 147.1,

152.3, 156.4, 165.1, 170.9; HRMS *m/z* Calcd for $C_{22}H_{23}N_3O_3$ $[M+H]^+$: 378.1818, Found: 378.1843.

*4.2.9. (E)-6-(3-oxo-3-(3-((m-tolyloxy)methyl)azetidin-1-yl)prop-1-en-1-yl)-3,4-dihydro-1,8-naphthyridin-2(1H)-one (**AEA9**)*

Yield = 27%; Yellow Solid; mp: 208–209 °C; IR (KBr, cm^{-1}): 3537, 2877, 1687, 1602, 1454, 1292, 1159, 977, 771, 688; ^{1}H NMR (400 MHz, DMSO-d_6): δ_H 10.64 (s, 1H), 8.34 (d, J = 2.0 Hz, 1H), 8.03 (s, 1H), 7.40 (d, J = 16.2 Hz, 1H), 7.16 (t, J = 7.8 Hz, 1H), 6.79–6.72 (m, 4H), 4.43–4.38 (m, 1H), 4.15–4.04 (m, 4H), 3.78–3.73 (m, 1H), 3.07–3.04 (m, 1H), 2.92–2.87 (m, 2H), 2.54–2.50 (m, 2H), 2.27 (s, 3H); ^{13}C NMR (500 MHz, DMSO-d_6): δ_C 21.0, 23.3, 27.6, 30.0, 49.9, 52.4, 68.9, 111.5, 115.1, 116.2, 119.0, 121.4, 125.3, 129.2, 133.5, 136.4, 138.9, 147.1, 152.3, 158.4, 165.0, 170.9; HRMS *m/z* Calcd for $C_{22}H_{23}N_3O_3$ $[M+H]^+$: 378.1818, Found: 378.1774.

*4.2.10. (E)-6-(3-oxo-3-(3-((p-tolyloxy)methyl)azetidin-1-yl)prop-1-en-1-yl)-3,4-dihydro-1,8-naphthyridin-2(1H)-one (**AEA10**)*

Yield = 32%; Pale brown solid; 210–211 °C; IR (KBr, cm^{-1}): 2875, 1689, 1602, 1510, 1359, 1292, 1242, 1193, 977, 815, 526; ^{1}H NMR (400 MHz, DMSO-d_6): δ_H 10.65 (s, 1H), 8.34 (d, J = 1.9 Hz, 1H), 8.02 (s, 1H), 7.39 (d, J = 15.6 Hz, 1H), 7.09 (t, J = 8.4 Hz, 2H), 6.85 (d, J = 8.8 Hz, 2H), 6.74 (d, J = 15.6 Hz, 1H), 4.40 (t, J = 8.8 Hz, 1H), 4.13–4.09 (m, 4H), 3.77–3.74 (m, 1H), 3.10–3.02 (m, 1H), 2.92–2.88 (m, 2H), 2.55–2.53 (m, 2H), 2.23 (s, 3H); ^{13}C NMR (500 MHz, DMSO-d_6): δ_C 20.0, 23.3, 27.6, 30.0, 40.9, 52.5, 69.1, 114.3, 116.2, 119.0, 125.3, 129.4, 129.8, 133.5, 136.4, 147.1, 152.3, 156.3, 165.0, 170.9; HRMS m/z Calcd for $C_{22}H_{23}N_3O_3$ $[M+H]^+$: 378.1818, Found: 378.1855.

*4.2.11. (E)-6-(3-(3-(naphthalen-2-yloxy)azetidin-1-yl)-3-oxoprop-1-en-1-yl)-3,4-dihydro-1,8-naphthyridin-2(1H)-one (**AEA11**)*

Yield = 23%; Brown solid; 250–251 °C; IR (KBr, cm^{-1}): 3197, 3059, 2875, 1681, 1598, 1442, 1215, 844, 756, 528; ^{1}H NMR (400 MHz, DMSO-d_6): δ_H 10.64 (brs, 1H), 8.35 (d, J = 1.0 Hz, 1H), 8.03 (s, 1H), 7.83 (d, J = 8.8 Hz, 1H), 7.80 (d, J = 8.3 Hz, 2H), 7.45 (d, J = 7.8 Hz, 1H), 7.41 (d, J = 15.6 Hz, 1H), 7.39–7.37 (m, 2H), 7.18 (dd, J = 2.4 Hz, 8.8 Hz, 1H), 6.76 (d, J = 15.6 Hz, 1H), 4.50–4.42 (m, 1H), 4.31 (d, J = 6.3 Hz, 2H), 4.22–4.10 (m, 2H), 3.88–3.80 (m, 1H), 3.20–3.10 (m, 1H), 2.91 (t, J = 7.9 Hz, 2H), 2.56–2.53 (m, 2H); ^{13}C NMR (500 MHz, DMSO-d_6): δ_C 23.3, 27.6, 30.0, 50.0, 52.5, 69.1, 106.9, 116.2, 118.5, 119.0, 123.6, 125.3, 126.4, 126.6, 127.4, 128.5, 129.3, 133.5, 134.2, 136.5, 147.1, 152.3, 156.3, 165.1, 170.9; HRMS *m/z* Calcd for $C_{25}H_{23}N_3O_3$ $[M+H]^+$: 414.1818; Found: 414.1840.

*4.2.12. (E)-6-(3-(3-(benzo[d]thiazol-2-yloxy)azetidin-1-yl)-3-oxoprop-1-en-1-yl)-3,4-dihydro-1,8-naphthyridin-2(1H)-one (**AEA12**)*

Yield = 36%; White solid; mp: 275–276 °C; IR (KBr, cm^{-1}): 3460, 2922, 1656, 1527, 1442, 1253, 1043, 761; ^{1}H NMR (400 MHz, DMSO-d_6): δ_H 10.65 (brs, 1H), 8.35 (s, 1H), 8.04 (s, 1H), 7.94 (d, J = 7.9 Hz, 1H), 7.69 (d, J = 7.9 Hz, 1H), 7.43 (d, J = 15.6 Hz, 1H), 7.43 (s, 1H), 7.32 (d, J = 7.6 Hz, 1H), 6.78 (d, J = 15.6 Hz, 1H), 5.63 (t, J = 3.2 Hz, 1H), 4.83–4.79 (m, 1H), 4.45–4.16 (m, 2H), 4.10–4.08 (m, 1H), 2.90 (t, J = 7.6 Hz, 2H), 2.54–2.50 (m, 2H); ^{13}C NMR (500 MHz, DMSO-d_6): δ_C 23.3, 29.9, 54.4, 57.2, 70.1, 116.2, 119.0, 120.7, 122.2, 124.0, 125.2, 126.3, 131.5, 133.6, 136.9, 147.3, 148.6, 152.4, 165.2, 170.6, 170.9; HRMS *m/z* Calcd for $C_{21}H_{18}N_4O_3S$ $[M+H]^+$: 407.1178, Found: 407.1165.

*4.2.13. (E)-6-(3-(3-(benzo[d]thiazol-2-ylmethyl)azetidin-1-yl)-3-oxoprop-1-en-1-yl)-3,4-dihydro-1,8-naphthyridin-2(1H)-one (**AEA13**)*

Yield = 23%; Pale brown solid; mp: 78–79 °C; IR (KBr, cm^{-1}): 3537, 3118, 2870, 1691, 1656, 1444, 1284, 1182, 773, 524; ^{1}H NMR (400 MHz, DMSO-d_6): δ_H 10.64 (brs, 1H), 8.33 (d, J = 1.5 Hz, 1H), 8.07 (d, J = 7.9 Hz, 1H), 8.03 (s, 1H), 7.95 (d, J = 7.9 Hz, 1H), 7.52–7.48 (m, 1H), 7.43 (d, J = 7.3 Hz, 1H), 7.39 (d, J = 15.8 Hz, 1H), 6.74 (d, J = 15.8 Hz, 1H), 4.46 (t, J = 8.5 Hz, 1H), 4.13 (t, J = 8.7 Hz, 2H), 3.79 (dd, J = 5.5 Hz, 10.1 Hz, 1H), 3.49 (d, J = 7.9 Hz, 2H), 3.22–3.16 (m, 1H), 2.89 (t, J = 7.6 Hz, 2H), 2.64–2.52 (m, 2H); ^{13}C NMR (500 MHz, DMSO-d_6): δ_C 23.2, 27.8, 30.0, 37.1, 52.5, 54.8, 116.3, 119.0, 122.0, 122.2, 124.9, 125.3, 126.1, 133.5, 134.6, 136.4, 147.2, 152.3, 152.7, 165.09, 169.0, 170.9; HRMS *m/z* Calcd for $C_{22}H_{20}N_4O_2S$ $[M+H]^+$: 405.1385, Found: 405.1386.

*4.2.14. (E)-6-(3-(3-(benzo[d]thiazol-2-yl)azetidin-1-yl)-3-oxoprop-1-en-1-yl)-3,4-dihydro-1,8-naphthyridin-2(1H)-one (**AEA14**)*

Yield = 25%; Brown solid; mp: 258–259 °C; IR (KBr, cm^{-1}): 3061, 2879, 1602, 1452, 1359, 1294, 1192, 1120, 979, 844, 761, 530; ^{1}H NMR (400 MHz, DMSO-d_6): δ_H 10.66 (brs, 1H), 8.37 (s, 1H), 8.12 (d, J = 7.6 Hz, 1H), 8.05 (s, 1H), 8.02 (d, J = 7.9 Hz, 1H), 7.55–7.52 (m, 1H), 7.46 (s, 1H), 7.45 (d, J = 15.9 Hz, 1H), 6.80 (d, J = 15.9 Hz, 1H), 4.85–4.75 (m, 1H), 4.75–4.55 (m, 1H), 4.50–4.35 (m, 2H), 4.25–4.15 (m, 1H), 2.91 (t, J = 7.4 Hz, 2H), 2.55–2.49 (m, 2H); ^{13}C NMR (400 MHz, DMSO-d_6): δ_C 23.3, 30.0, 31.6, 53.6, 55.6, 116.0, 119.0, 122.3, 122.5, 125.2, 126.3, 133.6, 134.7, 136.9, 137.8, 147.3, 152.4, 152.5, 165.3, 170.9, 171.5; HRMS *m/z* Calcd for $C_{21}H_{18}N_4O_2S$ $[M+H]^+$: 391.1229, Found: 391.1173.

*4.2.15. (E)-6-(3-(3-(3-methylbenzo[b]thiophen-2-yl)azetidin-1-yl)-3-oxoprop-1-en-1-yl)-3,4-dihydro-1,8-naphthyridin-2(1H)-one (**AEA15**)*

Yield = 23%; White solid; mp: 255–256 °C; IR (KBr, cm^{-1}): 3018, 1656, 1462, 1215, 1190, 756, 669; ^{1}H NMR (400 MHz, DMSO-d_6): δ_H 10.66 (brs, 1H), 8.37 (s, 1H), 8.04 (s, 1H), 7.94 (d, J = 7.8 Hz, 1H), 7.72 (d, J = 7.8 Hz, 1H), 7.46 (d, J = 15.6 Hz, 1H), 7.41–7.33 (m, 2H), 6.80 (d, J = 15.6 Hz, 1H), 4.82 (d, J = 7.8 Hz, 1H), 4.51–4.41 (m, 2H), 4.35 (d, J = 8.3 Hz, 1H), 4.00–3.99 (m, 1H), 2.94–2.89 (m, 2H), 2.66–2.53 (m, 2H), 2.32 (s, 3H); ^{13}C NMR (400 MHz, DMSO-d_6): δ_C 11.4, 23.3, 27.4, 30.0, 55.4, 57.5, 113.8, 116.1, 116.6, 119.1, 121.7, 122.5, 124.3, 125.3, 128.1, 133.79, 137.0, 147.2, 152.4, 158.2, 158.6, 165.2, 171.0; HRMS *m/z* Calcd for $C_{23}H_{21}N_3O_2S$ $[M+H]^+$: 404.1433, Found: 404.1394.

*4.2.16. (E)-6-(3-(3-(3-methylbenzofuran-2-yl)azetidin-1-yl)-3-oxoprop-1-en-1-yl)-3,4-dihydro-1,8-naphthyridin-2(1H)-one (**AEA16**)*

Yield = 20%; White solid; mp: 236–237 °C; IR (KBr, cm^{-1}): 3128, 2881, 1691, 1651, 1454, 1192, 979, 748, 675, 526; ^{1}H NMR (400 MHz, DMSO-d_6): δ_H 10.66 (brs, 1H), 8.37 (s, 1H), 8.03 (s, 1H), 7.56–7.53 (m, 2H), 7.47 (d, J = 15.6 Hz, 1H), 7.28–7.24 (m, 2H), 6.80 (d, J = 15.6 Hz, 1H), 4.75–4.62 (m, 1H), 4.54–4.48 (m, 1H), 4.40–4.32 (m, 1H), 4.31–4.21 (m, 1H), 4.18–4.10 (m, 1H), 2.91 (t, J = 7.9 Hz, 2H), 2.56–2.52 (m, 2H), 2.19 (s, 3H); ^{13}C NMR (400 MHz, DMSO-d_6): δ_C 7.5, 23.3, 24.6, 30.0, 52.4, 54.4, 110.8, 111.4, 116.1, 119.1, 119.3, 122.5, 124.1, 125.3, 129.6, 133.7, 136.9, 147.3, 151.6, 152.5, 153.4, 165.2, 171.0; HRMS *m/z* Calcd for $C_{23}H_{21}N_3O_3$ $[M+H]^+$: 388.1661, Found: 388.1685.

*4.2.17. (E)-6-(3-(3-(5-methoxy-3-methylbenzofuran-2-yl)azetidin-1-yl)-3-oxoprop-1-en-1-yl)-3,4-dihydro-1,8-naphthyridin-2(1H)-one (**AEA17**)*

Yield = 16%; White solid; mp: 238–239 °C; IR (KBr, cm^{-1}): 3745, 2924, 1656, 1462, 1192, 833, 723; ^{1}H NMR (400 MHz, DMSO-d_6): δ_H 10.66 (brs, 1H), 8.37 (s, 1H), 8.03 (s, 1H), 7.46 (d, J = 15.6 Hz, 1H), 7.44 (d, J = 8.8 Hz, 1H), 7.04 (d, J = 2.4 Hz, 1H), 6.85 (dd, J = 2.5 Hz, 8.8 Hz, 1H), 6.79 (d, J = 15.6 Hz, 1H), 4.67 (t, J = 8.6 Hz, 1H), 4.49–4.45 (m, 1H), 4.33 (t, J = 9.2 Hz, 1H), 4.26–4.19 (m, 1H), 4.12–4.08 (m, 1H), 3.79 (s, 3H), 2.91 (t, J = 7.6 Hz, 2H), 2.55–2.50 (m, 2H), 2.16 (s, 3H); ^{13}C NMR (400 MHz, DMSO-d_6): δ_C 7.5, 23.3, 24.7, 30.0, 52.4, 54.4, 55.6, 111.3, 111.6, 112.3, 113.7, 116.2, 116.6, 119.1, 125.3, 130.3, 133.8,

136.9, 147.1, 152.4, 155.5, 158.6, 165.22, 171.0; HRMS *m/z* Calcd for $C_{24}H_{23}N_3O_4$ $[M+H]^+$: 418.1767, Found: 418.1731.

4.2.18. (E)-6-(3-(3-(5-chloro-3-methylbenzofuran-2-yl)azetidin-1-yl)-3-oxoprop-1-en-1-yl)-3,4-dihydro-1,8-naphthyridin-2(1H)-one (**AEA18**)

Yield = 14%; White solid; mp: 261–262 °C; IR (KBr, cm^{-1}): 2949, 1689, 1602, 1444, 1190, 977, 750, 526; ^1H NMR (400 MHz, DMSO-d_6): δ_H 10.66 (brs, 1H), 8.37 (s, 1H), 8.03 (s, 1H), 7.63 (s, 1H), 7.59 (d, J = 8.8 Hz, 1H), 7.46 (d, J = 15.8 Hz, 1H), 7.30 (dd, J = 1.6 Hz, 8.5 Hz, 1H), 6.78 (d, J = 15.8 Hz, 1H), 4.68 (t, J = 8.5 Hz, 1H), 4.51–4.46 (m, 1H), 4.37–4.25 (m, 2H), 4.14–4.10 (m, 1H), 2.91 (t, J = 7.5 Hz, 2H), 2.54–2.51 (m, 2H), 2.17 (s, 3H); ^{13}C NMR (500 MHz, DMSO-d_6): δ_C 7.3, 23.3, 24.6, 30.0, 52.3, 54.3, 111.4, 112.4, 116.1, 118.9119.0, 123.9, 125.2, 127.0, 131.3, 133.6, 136.9, 147.2, 151.9, 152.4, 153.5, 165.1, 170.9; HRMS *m/z* Calcd for $C_{23}H_{20}ClN_3O_3$ $[M+H]^+$: 422.1271, Found: 422.1289.

4.2.19. (E)-6-(3-(3-(4-methylquinolin-2-yl)azetidin-1-yl)-3-oxoprop-1-en-1-yl)-3,4-dihydro-1,8-naphthyridin-2(1H)-one (**AEA19**)

Yield = 18%; Brown solid; mp: 223–224 °C; IR (KBr, cm^{-1}): 3061, 1651, 1598, 1489, 1290, 1190, 972, 848, 769, 526; ^1H NMR (400 MHz, DMSO-d_6): δ_H 10.65 (brs, 1H), 8.36 (d, J = 1.5 Hz, 1H), 8.08 (d, J = 7.8 Hz, 1H), 8.05 (s, 1H), 8.00 (d, J = 8.3 Hz, 1H), 7.82–7.73 (m, 1H), 7.63–7.59 (m, 1H), 7.46–7.41 (m, 2H), 6.81 (d, J = 15.6 Hz, 1H), 4.73–4.63 (m, 2H), 4.41–4.37 (m, 1H), 4.24–4.15 (m, 2H), 2.91 (t, J = 7.6 Hz, 2H), 2.69 (s, 3H), 2.55–2.53 (m, 2H); ^{13}C NMR (500 MHz, DMSO-d_6): δ_C 18.1, 23.3, 30.0, 34.4, 52.9, 54.7, 116.3, 119.0, 121.0, 124.1, 125.3, 126.0, 126.7, 129.0, 129.4, 133.6, 136.6, 145.0, 147.0, 147.2, 152.4, 160.5, 165.2, 170.9; HRMS *m/z* Calcd for $C_{24}H_{22}N_4O_2$ $[M+H]^+$: 399.1821, Found: 399.1833.

4.2.20. (E)-6-(3-oxo-3-(3-(pyridin-2-yl)azetidin-1-yl)prop-1-en-1-yl)-3,4-dihydro-1,8-naphthyridin-2(1H)-one (**AEA20**)

Yield = 23%; Brown solid; mp: 222–223 °C; IR (KBr, cm^{-1}): 3007, 2877, 2677, 1687, 1597, 1433, 1357, 1188, 779, 530; ^1H NMR (400 MHz, DMSO-d_6): δ_H 10.67 (brs, 1H), 8.61 (d, J = 4.4 Hz, 1H), 8.36 (s, 1H), 8.03 (s, 1H), 7.80–7.76 (m, 1H), 7.42 (d, J = 15.6 Hz, 1H), 7.37 (d, J = 7.8 Hz, 1H), 7.30 (dd, J = 5.1 Hz, 7.1 Hz, 1H), 6.77 (d, J = 15.6 Hz, 1H), 4.65 (t, J = 8.0 Hz, 1H), 4.48–4.45 (m, 1H), 4.46 (t, J = 8.8 Hz, 1H), 4.10–3.99 (m, 2H), 3.09 (dt, J = 7.3 Hz, 12.2 Hz, 2H), 2.90 (t, J = 7.6 Hz, 2H); ^{13}C NMR (400 MHz, DMSO-d_6): δ_C 23.3, 30.0, 33.9, 53.4, 55.4, 116.2, 119.0, 122.2, 122.4, 125.3, 133.6, 136.5, 136.8, 147.1, 149.4, 152.4, 160.3, 165.1, 170.9; HRMS *m/z* Calcd for $C_{19}H_{18}N_4O_2$ $[M+H]^+$: 335.1508, Found: 335.1515.

4.2.21. (E)-6-(3-oxo-3-(3-phenylazetidin-1-yl)prop-1-en-1-yl)-3,4-dihydro-1,8-naphthyridin-2(1H)-one (**AEA21**)

Yield = 50%; Off-white Solid; mp: 268–269 °C; IR (KBr, cm^{-1}): 3034, 2875, 1656, 1591, 1365, 1290, 1193, 758, 700; ^1H NMR (400 MHz, DMSO-d_6): δ_H 10.65 (s, 1H), 8.35 (d, J = 2.0 Hz, 1H), 8.02 (d, J = 0.9 Hz, 1H), 7.43 (d, J = 15.7 Hz, 1H), 7.38–7.36 (m, 4H), 7.35–7.25 (m, 1H), 6.77 (d, J = 15.6 Hz, 1H), 4.71 (t, J = 8.3 Hz, 1H), 4.39–4.27 (m, 2H), 3.95–3.89 (m, 2H), 2.93–2.89 (m, 2H), 2.56–2.51 (m, 2H); ^{13}C NMR (400 MHz, DMSO-d_6): δ_C 23.3, 30.0, 32.6, 54.8, 56.9, 116.3, 119.0, 125.3, 126.7, 128.6, 133.5, 136.5, 136.8, 142.1147.1, 147.7, 165.1, 170.9; HRMS *m/z* Calcd for $C_{20}H_{19}N_3O_2$ $[M+H]^+$: 334.1556, Found: 334.1557.

4.2.22. (E)-N-(5-(3-(3-(3-methylbenzofuran-2-yl)azetidin-1-yl)-3-oxoprop-1-en-1-yl)pyridin-2-yl)acetamide (**AEA22**)

Yield = 15%; White solid; mp: 226–227 °C; IR (KBr, cm^{-1}): 3255, 2949, 2883, 1651, 1519, 1444, 1301, 975, 837, 744, 624; ^1H NMR (400 MHz, DMSO-d_6): δ_H 10.67 (s, 1H), 8.61 (d, J = 1.9 Hz, 1H), 8.14–8.08 (m, 1H), 8.11 (m, 1H), 7.56–7.53 (m, 2H), 7.49 (d, J = 15.7 Hz, 1H), 7.28–7.24 (m, 2H), 6.84 (d, J = 15.7 Hz, 1H), 4.71–4.67 (m, 1H), 4.52–4.48 (m, 1H), 4.37–4.33 (m, 1H), 4.30–4.23 (m, 1H), 4.15–4.11 (m, 1H), 2.18 (s, 3H), 2.10 (s, 3H); ^{13}C NMR (400 MHz, DMSO-d_6): δ_C 7.4, 23.9, 24.6, 52.4, 54.4, 110.8, 111.3, 112.8, 116.7, 119.2, 122.4, 124.1, 126.1, 129.6, 136.5, 136.6, 148.5, 151.5, 152.7, 153.4, 165.0, 169.4; HRMS *m/z* Calcd for $C_{22}H_{21}N_3O_3$ $[M+H]^+$:376.1661, Found: 376.1678.

4.2.23. (E)-N-(5-(3-(3-(3-methylbenzofuran-2-yl)azetidin-1-yl)-3-oxoprop-1-en-1-yl)pyridin-2-yl)-2-(1H-1,2,3-triazol-1-yl) acetamide (**AEA23**)

Yield = 24%; Pale yellow solid; mp: 227–228 °C; IR (KBr, cm^{-1}): 3321, 2951, 1697, 1537, 1390, 1305, 744; ^1H NMR (400 MHz, DMSO-d_6): δ_H 11.21 (s, 1H), 8.68 (d, J = 1.9 Hz, 1H), 8.20 (dd, J = 2.5 Hz, 8.8 Hz, 1H), 8.16 (s, 1H), 8.03 (d, J = 8.3 Hz, 1H), 7.77 (s, 1H), 7.56–7.54 (m, 2H), 7.51 (d, J = 15.6 Hz, 1H), 7.30–7.22 (m, 2H), 6.89 (d, J = 15.6 Hz, 1H), 5.46 (s, 2H), 4.72–4.67 (m, 1H), 4.52–4.48 (m, 1H), 4.38–4.33 (m, 1H), 4.29–4.23 (m, 1H), 4.16–4.12 (m, 1H), 2.19 (s, 3H); ^{13}C NMR (500 MHz, DMSO-d_6): δ_C 7.4, 24.6, 51.9, 52.4, 54.4, 110.8, 111.3, 113.1, 117.2, 119.2, 122.4, 124.1, 126.5, 126.8, 129.6, 133.1, 136.4, 136.8, 148.7, 151.5, 152.0, 153.4, 164.9, 165.4; HRMS *m/z* Calcd for $C_{24}H_{22}N_6O_3$ $[M+H]^+$:443.1832, Found: 443.1816.

4.2.24. (E)-6-(3-(3-(3-methylbenzofuran-2-yl)azetidin-1-yl)-3-oxoprop-1-en-1-yl)-3-(2-morpholinoethyl)-3,4-dihydropyrido[2,3-d]pyrimidin-2(1H)-one (**AEA24**)

Yield = 13%; Off-white solid; mp: 218–219 °C; (KBr, cm^{-1}): 2949, 2818, 1672, 1593, 1492, 1450, 1408, 1296, 1114, 746; ^1H NMR (400 MHz, DMSO-d_6): δ_H 9.88 (brs, 1H), 8.35 (s, 1H), 7.93 (s, 1H), 7.56–7.53 (m, 2H), 7.45 (d, J = 15.8 Hz, 1H), 7.30–7.23 (m, 2H), 6.74 (d, J = 15.5 Hz, 1H), 4.67 (t, J = 8.5 Hz, 1H), 4.54 (s, 2H), 4.50–4.47 (m, 1H), 4.36–4.33 (m, 1H), 4.29–4.25 (m, 1H), 4.14–4.11 (m, 1H), 3.60–3.50 (m, 4H), 3.45 (t, J = 6.1 Hz, 2H), 2.41–2.35 (m, 6H), 2.19 (s, 3H); ^{13}C NMR (500 MHz, DMSO-d_6): δ_C 7.4, 24.6, 40.0, 46.9, 52.4, 53.2, 54.3, 55.4, 65.9, 110.8, 111.3, 113.4, 115.5, 119.2, 122.4, 124.1, 124.5, 129.6, 131.7, 136.9, 148.2, 151.2, 151.5, 152.8, 153.4, 165.1; HRMS *m/z* Calcd for $C_{28}H_{31}N_5O_4$ $[M+H]^+$: 502.2454, Found: 502.2432.

4.3. General procedure for the synthesis of **AEA25–28**

To a stirred suspension of bromo derivative **30** or **31** or **32** or **33** (1 equiv), acrylamide **29** (1.3 equiv) in propionitrile:DMF (4:1 volumes) was added diisopropyl ethyl amine (3 equiv) and the reaction mixture was degassed with nitrogen for 10 min. Then $Pd(OAc)_2$ (0.2 equiv), P(o-tolyl)$_3$ (0.4 equiv) were added, again degassed with nitrogen for another 10 min and the reaction mixture was allowed to stir at 110 °C for 16 h. The reaction mixture was cooled to room temperature, filtered through celite and filtrate was evaporated under vacuum. The resulting residue was diluted with H_2O (50 volumes) and extracted with ethyl acetate (3 × 50 volumes). The combined organic layers were washed with brine (50 volumes), dried over Na_2SO_4, filtered and volatiles were removed under vacuum. The crude residue was purified by column chromatography to furnish the desired products **AEA25–28**.

4.3.1. (E)-7-(3-(3-(3-methylbenzofuran-2-yl)azetidin-1-yl)-3-oxoprop-1-en-1-yl)-4,5-dihydro-1H-pyrido[2,3-e][1,4]diazepin-2(3H)-one (**AEA25**)

Yield = 10%; Pale yellow solid; mp: 204–205 °C; IR (KBr, cm^{-1}): 3280, 3062, 2912, 2883, 1651, 1454, 1328, 977, 856, 748; ^1H NMR (400 MHz, DMSO-d_6): δ_H 10.07 (brs, 1H), 8.45 (d, J = 2.0 Hz, 1H), 7.98 (s, 1H), 7.56–7.53 (m, 2H), 7.47 (d, J = 15.7 Hz, 1H), 7.30–7.22 (m, 2H), 6.83 (d, J = 16.2 Hz, 1H), 4.69 (t, J = 8.5 Hz, 1H), 4.52–4.48

(m, 1H), 4.35 (t, J = 9.3 Hz, 1H), 4.30–4.23 (m, 1H), 4.15–4.11 (m, 1H), 3.90 (s, 2H), 3.63 (s, 2H), 3.06 (brs, 1H), 2.19 (s, 3H); ^{13}C NMR (400 MHz, DMSO-d_6): δ_C 7.4, 24.6, 50.3, 52.4, 54.4, 55.1, 110.8, 111.3, 116.7, 119.3, 122.4, 124.1, 125.2, 126.5, 129.6, 135.4, 136.4, 147.1, 151.0, 151.5, 153.4, 165.1, 174.5; HRMS m/z Calcd for $C_{23}H_{22}N_4O_3$ $[M+H]^+$: 403.1770, Found: 403.1757.

4.3.2. (E)-4-methyl-7-(3-(3-(3-methylbenzofuran-2-yl)azetidin-1-yl)-3-oxoprop-1-en-1-yl)-4,5-dihydro-1H-pyrido[2,3-e][1,4] diazepin-2(3H)-one (**AEA26**)

Yield = 44%; Pale green solid; mp: 218–219 °C; IR (KBr, cm^{-1}): 3062, 2945, 2879, 1651, 1454, 1344, 850, 742, 663; ^{1}H NMR (400 MHz, DMSO-d_6): δ_H 10.38 (brs, 1H), 8.54 (s, 1H), 8.11 (s, 1H), 7.56–7.54 (m, 2H), 7.50 (d, J = 15.6 Hz, 1H), 7.30–7.22 (m, 2H), 6.86 (d, J = 15.6 Hz, 1H), 4.70 (t, J = 8.6 Hz, 1H), 4.53–4.49 (m, 1H), 4.36 (t, J = 9.0 Hz, 1H), 4.29–4.26 (m, 1H), 4.15–4.12 (m, 1H), 3.80 (s, 2H), 3.44 (s, 2H), 2.37 (s, 3H), 2.19 (s, 3H); ^{13}C NMR (400 MHz, DMSO-d_6): δ_C 7.4, 24.6, 42.3, 52.4, 54.4, 56.8, 60.3, 110.8, 111.3, 117.2, 119.2, 122.4, 123.0, 124.1, 126.1, 129.6, 136.2, 137.0, 148.0, 151.5, 151.8, 153.4, 165.0, 171.4; HRMS m/z Calcd for $C_{24}H_{24}N_4O_3$ $[M+H]^+$:417.1927, Found: 417.1877.

4.3.3. (E)-7-(3-(3-(3-methylbenzofuran-2-yl)azetidin-1-yl)-3-oxoprop-1-en-1-yl)-4-(2-morpholinoethyl)-4,5-dihydro-1H-pyrido [2,3-e][1,4]diazepin-2(3H)-one (**AEA27**)

Yield = 23%; Pale yellow solid; mp: 240–241 °C; IR (KBr, cm^{-1}): 3059, 2947, 2812, 1658, 1454, 1114, 854, 746; ^{1}H NMR (400 MHz, DMSO-d_6): δ_H 10.32 (s, 1H), 8.52 (d, J = 2.0 Hz, 1H), 8.10 (d, J = 2.0 Hz, 1H), 7.56–7.53 (m, 1H), 7.49 (d, J = 15.9 Hz, 1H), 7.26–7.24 (m, 2H), 6.86 (d, J = 15.9 Hz, 1H), 4.68–4.64 (m, 1H), 4.52–4.48 (m, 1H), 4.39–4.36 (m, 2H), 4.28–4.20 (m, 1H), 4.18–4.16 (m, 2H), 3.91 (s, 2H), 3.53 (s, 2H), 3.52–3.51 (m, 3H), 3.29 (s, 2H), 2.67–2.65 (m, 2H), 2.42–2.40 (m, 2H), 2.33–2.31 (m, 2H), 2.19 (s, 3H); ^{13}C NMR (400 MHz, DMSO-d_6): δ_C 7.4, 24.6, 50.2, 52.4, 53.4, 54.4, 55.2, 56.3, 59.1, 66.0, 110.8, 111.3, 117.1, 119.2, 122.4, 123.1, 124.1, 125.9, 129.6, 136.3, 137.1, 147.9, 151.5, 151.7, 153.4, 165.0, 172.1; HRMS m/z Calcd for $C_{29}H_{33}N_5O_4$ $[M+H]^+$: 516.2611, Found: 516.2665.

4.3.4. (E)-8-(3-(3-(3-methylbenzofuran-2-yl)azetidin-1-yl)-3-oxoprop-1-en-1-yl)-2,3-dihydro-1H-pyrido[2,3-b][1,4]diazepin-4(5H)-one (**AEA28**)

Yield = 31%; Pale brown solid; mp: 301–302 °C; IR (KBr, cm^{-1}): 3302, 3066, 2947, 2881, 1656, 1585, 1452, 1382, 850, 744; ^{1}H NMR (400 MHz, DMSO-d_6): δ_H 9.75 (s, 1H), 7.99 (d, J = 1.5 Hz, 1H), 7.56–7.52 (m, 2H), 7.39 (d, J = 15.6 Hz, 1H), 7.36 (d, J = 1.9 Hz, 1H), 7.30–7.22 (m, 2H), 6.65 (d, J = 15.6 Hz, 1H), 6.07 (t, J = 3.6 Hz, 1H), 4.68 (t, J = 8.5 Hz, 1H), 4.51–4.46 (m, 1H), 4.35 (t, J = 9.3 Hz, 1H), 4.30–4.24 (m, 1H), 4.13 (dd, J = 5.9 Hz, 9.3 Hz, 1H), 3.44–3.40 (m, 2H), 2.61 (t, J = 5.4 Hz, 2H), 2.19 (s, 3H); ^{13}C NMR (500 MHz, DMSO-d_6): δ_C 7.4, 24.6, 37.7, 42.2, 52.4, 54.3, 110.8, 111.3, 116.3, 119.2, 122.4, 122.7, 124.1, 126.5, 129.6, 135.0, 136.9, 137.4, 140.0, 151.4, 153.3, 164.9, 172.1; HRMS m/z Calcd for $C_{23}H_{22}N_4O_3$ $[M+H]^+$: 403.1770, Found: 403.1803.

4.4. S. aureus FabI biochemical assay

The enzymatic assay [17] is based on the decrease in absorbance at 340 nm resulting from the oxidation of NADPH accompanying the reduction of enoyl − ACP, catalysed by FabI enzyme. The assay was carried out in 100 mM Sodium ADA (N-[2-Acetamido] iminodiacetic acid) buffer, pH 6.5. FabI enzyme (2400 ng/assay) was pre-incubated with NADH (375 μM) and test compounds for 30 min and the reaction was started by adding Crotonoyl CoA (250 μM). The total reaction volume was 100 μL. After 2 h incubation at room temperature, the absorbance at 340 nm was measured and the enzyme activity was determined. Test compounds were initially screened at 1 μM, in duplicate. Dose–response studies were subsequently carried out for active compounds. IC_{50} values were determined by fitting the activity data at different concentrations of the compound to sigmoidal dose response (variable slope) curve fitting program using GraphPad Prism software V5. The standard error in IC_{50} values estimated from the curve fitting was <15%.

4.5. In vitro antibacterial screen

Minimum Inhibitory Concentration (MIC) was determined by broth microdilution method as per CLSI guidelines. Serial two-fold dilution of the compounds was made using MHB in 96 well microtitre plates at twice the desired final concentration. 50 μL of the adjusted inoculum suspension was dispensed into each well to give a final inoculum density of 5×10^5 CFU/mL. Broth, compound and organism controls were set up in duplicate. *S. aureus* ATCC 29213 was incorporated as a quality control strain in the study. Plates were incubated at 35 ± 2 °C for 16–20 h in an ambient air incubator. After the incubation period, growth of organism in the wells was detected by unaided eye facilitated by a viewing device. The amount of growth in the wells containing the antibiotic was compared with the amount of growth in organism control wells (no antibiotic) to help in determining the end point. MIC was the lowest concentration of the antibiotic/compound which inhibits bacterial growth as detected by unaided eye and expressed as μg/mL.

4.6. Protein expression, purification and co-crystallization of E. coli FabI [37]

Gene sequence corresponding to full length *E. coli* FabI was cloned into pET28a vector. Transformants of *E. coli* BL21DE3 containing pET28a-Ec FabI were grown to an optical density (595 nm) of 0.8 and induced with 0.5 mM IPTG at 18 °C for 18 h. Cell pellet was resuspended in lysis buffer containing 50 mM Tris pH 7.5, 500 mM NaCl, 1 mM DTT, 50 μg/μL Lysozyme, cells lysed with sonication and clarified lysate passed through Ni-NTA column. Protein was eluted with buffer containing 50 mM Tris pH 7.5, 500 mM NaCl, 1 mM DTT and 250 mM imidazole. Fractions containing *E. coli* FabI were pooled and passed through Superdex-75 gel filtration column. Fractions containing pure FabI protein were incubated with 5 M excess of inhibitor and 2 M excess of NADH for 1 h at 4 °C. After, incubation protein was concentrated to 16 mg/mL for crystallization experiments. Crystals were grown at 20 °C using hanging drop vapour diffusion method. Crystallization well buffer contained 0.1 M sodium acetate pH 4.6, 12% PEG 4000 and 200 mM ammonium acetate. One microlitre protein solution was mixed with one microlitre of crystallization well buffer containing 0.1 M sodium acetate pH 4.6, 12% PEG 4000 and 200 mM ammonium acetate. Crystals with the dimensions of 0.1 × 0.05 × 0.05 mm were obtained overnight.

4.7. X-ray crystallography

The co-crystals were flash frozen at 100 K using 20% glycerol as cryo-protectant. The diffraction data sets were collected using in-house Rigaku RU300 X-ray generator with R-AXIS IV++ detector to a maximum resolution of 3.2 Å. Data indexing, integration and scaling were performed using DENZO and SCALEBPCK [38]. The structure was solved by molecular replacement (MR) method using the PDB code 1C14 as the template search model. Alternate cycles of restrained refinement and manual rebuilding were performed with the programs REFMAC 5.2.0001 [39,40] and Coot [41] respectively. 5% of the reflections were randomly excluded from the refinement to monitor the free residual-factor (R_{free}). A summary of the data reduction and

structure refinement statistics is provided in supplementary material. Coordinates of the X-ray structure have been deposited in the Protein Data Bank with accession codes 4JQC (AFN-1252) and 4JX8 (AEA16). Figures showing structural models were rendered using PyMOL [42]. Inhibitors could be modelled into the electron density unambiguously near the active site. Figure depicting the electron density map is shown in the supplementary information.

4.8. Metabolic stability study in mice liver microsomes

In vitro metabolism of compounds was studied in mouse liver microsomes to assess the metabolic stability at 1 μM concentration. The typical reaction mixture consists of incubation buffer (KH_2PO_4, pH 7.4), protein (liver microsomes, assay concentration: 0.3 mg/mL), NADPH (assay concentration: 1 mM) and test compound. Reaction was initiated by the addition of 20 μL of NADPH. Reaction mixture was incubated at 37 °C in a water bath. Reactions were terminated at designated time points (0, 15 and 60 min) by adding 100 μL of acetonitrile containing internal standard (carbamazapine – 0.5 μg/mL) and contents were extracted by cyclo-mixing for 2 min. This mixture was centrifuged for 5 min at 13,000 rpm and 180 μL of the clear supernatant was separated. An aliquot of 20 μL of the sample was injected onto LC-MS/MS for analysis. The percentage of parent remaining at the termination of reaction was quantified.

4.9. In vivo pharmacokinetic study protocol

The male Swiss albino mice (CD-1) ($n = 8–9$), weighing between 25 and 35 g were used to determine the pharmacokinetic parameters of test compounds. The oral pharmacokinetics study was conducted under fasted condition (~4 h) and animals had free access to water. Test compound was administered by oral gavage at dose of 10 mg/kg as a suspension. The excipients used for the formulation was 0.25% Tween 80 and 0.225% of sodium carboxy methyl cellulose. Blood samples (0.25 mL) were collected from retro-orbital plexus at designated time points (sparse sampling, $n = 3$ per time point) into micro centrifuge tubes containing 10 μL of EDTA and centrifuged at 13,000 rpm for 4 min. The supernatant plasma was stored at −20 °C until analysis. The samples were analysed for test compound concentration using a suitable LC-MS/MS method. The pharmacokinetic parameters of test compound were calculated by non-compartmental analysis using WinNonlin® Professional Version 5.2.

4.10. In vivo efficacy study protocol

All in vivo experiments were approved by the institutional animal ethics committee (IAEC). Female and male CD1 mice, 4–6 weeks old, weighing 20 ± 2 g were used in the study. Organisms were sub-cultured on Columbia blood agar (CBA) media and incubated at 35 ± 2 °C for 18–24 h. Inoculum was prepared in normal saline and further diluted with mucin to achieve final concentration of 5% (w/v). Three doses were tested per compound and/or standard drug using 6 animals per dose group (3 males, 3 females). Each mice was administered 0.5 mL of inoculum (cfu $2–3 \times 10^8$ cfu/animal) by intra-peritoneal route. One group of mice was not treated and served as untreated control (UTC). Respective vehicle control groups were also included. Test compounds and standard antibiotics were formulated in Tween 80 + 0.25% CMC for oral administration and were administered as *b.i.d.* at 1 h and 4 h post infection. Animals were monitored for 5 days and end point was determined by survival/death in each treated and untreated groups. The ED_{50} was calculated by non-linear regression analysis using GraphPad Prism software V5.

Acknowledgements

We appreciate the services extended by the Analytical Research department of Aurigene Discovery Technologies for having carried out all the analytical work. NAR, RY, IA and YKL acknowledge the support from the University of Malaya, Malaysia.

Appendix A. Supplementary data

Supplementary data related to this article can be found at http://dx.doi.org/10.1016/j.ejmech.2014.07.036.

References

[1] C.A. Loffler, C. MacDougall, Update on prevalence and treatment of methicillin-resistant *Staphylococcus aureus* infections, Expert Rev. Anti-infect. Ther. 5 (2007) 961–981.
[2] S.J. Projan, Why is big pharma getting out of antibacterial drug discovery? Curr. Opin. Microbiol. 6 (2003) 427–430.
[3] S.W. White, J. Zheng, Y. Zhang, C.O. Rock, The structural biology of type II fatty acid biosynthesis, Annu. Rev. Biochem. 74 (2005) 791–831.
[4] H. Lu, P. Tonge, Inhibitors of FabI, an enzyme drug target in the bacterial fatty acid biosynthesis pathway, J. Acc. Chem. Res. 41 (2008) 11–20.
[5] H. Xu, T.J. Sullivan, J. Sekiguchi, T. Kirikae, I. Ojima, C.F. Stratton, W. Mao, F.L. Rock, M.R.K. Alley, F. Johnson, S.G. Walker, P.J. Tonge, Mechanism and inhibition of *S. a* FabI, the enoyl reductase from *Staphylococcus aureus*, Biochemistry 47 (2008) 4228–4236.
[6] J. Schiebel, A. Chang, H. Lu, M.V. Baxter, P.J. Tonge, C. Kisker, *Staphylococcus aureus* FabI: inhibition, substrate recognition and potential implications for in vivo essentiality, Structure 20 (2012) 802–813.
[7] K.H. Kim, B.H. Ha, S.J. Kim, S.K. Hong, K.Y. Hwang, E.E. Kim, Crystal structures of enoyl-ACP reductases I (FabI) and III (FabL) from *B. subtilis*, J. Mol. Biol. 406 (2011) 403–415.
[8] L. Zhu, J. Lin, J. Ma, J.E. Cronan, H. Wang, Triclosan resistance of *Pseudomonas aeruginosa* PAO1is due to FabV, a triclosan resistant enoyl-acyl carrier protein reductase, Antimicrob. Agents Chemother. 54 (2010) 689–698.
[9] M.A. Seefeld, W.H. Miller, K.A. Newlander, W.J. Burgess, W.E. DeWolf, P.A. Elkins, M.S. Head, D.R. Jakas, C.A. Janson, P.M. Keller, P.J. Manley, D.A. Heerding, G. Chan, A.P. Fosberry, D.D. Jaworski, T.D. Moore, D.J. Payne, S. Pearson, B.J. Polozzi, X. Qiu, S.F. Rittenhouse, I.N. Uzinkas, N.G. Wallis, W.F. Huffman, Indole-naphthyridinone as inhibitors of bacterial enoyl-ACP reductases FabI and FabK, J. Med. Chem. 46 (2003) 1627–1635.
[10] J. Ramnauth, M.D. Surman, P.B. Sampson, B. Forrest, J. Wilson, E. Freeman, D.D. Manning, F. Martin, A. Toro, M. Domagala, D.E. Awrey, E. Bardouniotis, N. Kaplan, J. Berman, H.W. Pauls, 2,34,5-Tetrahydro-1H-pyrido[2,4-b and e][1,4] diazepines as inhibitors of the bacterial enoyl ACP reductase FabI, Bioorg. Med. Chem. Lett. 19 (2009) 5359–5362.
[11] P.B. Sampson, C. Picard, S. Handerson, T.E. McGrath, M. Domagala, A. Leeson, V. Romanov, D.E. Awrey, D. Thambipillai, E. Bardouniotis, N. Kaplan, J.M. Berman, H.W. Pauls, Spiro-naphthyridinone piperidines as inhibitors of *S. aureus* and *E. coli* enoyl-ACP reductase (FabI), Bioorg. Med. Chem. Lett. 19 (2009) 5355–5358.
[12] M.A. Seefeld, W.H. Miller, K.A. Newlander, W.J. Burgess, D.J. Payne, S.F. Rittenhouse, T.D. Moore, W.E. DeWolf Jr., P.M. Keller, X. Qiu, C.A. Janson, K. Vaidya, A.P. Fosberry, M.G. Smyth, D.D. Jawroski, C. Slater-Radosti, W.F. Huffman, Inhibitors of bacterial enoyl acyl carrier protein reductase (FabI): 2,9-disubstituted 1,2,3,4-tetrahydropyrido[3,4]indoles as potential antibacterial agents, Bioorg. Med. Chem. Lett. 11 (2001) 2241–2244.
[13] H. Kitagawa, T. Ozava, S. Takahata, M. Iida, M. Yamada, Phenylimidazole derivatives of 4-pyridone as dual inhibitors of bacterial enoyl-acyl carrier protein reductases FabI and FabK, J. Med. Chem. 50 (2007) 4710–4720.
[14] H. Kitagawa, K. Kumura, S. Takahata, M. Iida, K. Atsumi, 4-Pyridone derivatives as new inhibitors of bacterial enoyl-ACP reductase FabI, Bioorg. Med. Chem. Lett. 15 (2007) 1106–1116.
[15] M. Chhibber, G. Kumar, P. Parasuraman, T.N. Ramya, N. Surolia, A. Surolia, Novel diphenyl ethers: design, docking studies, synthesis and inhibition of enoyl ACP reductase of *Plasmodium falciparum* and *Escherichia coli*, Bioorg. Med. Chem. 14 (2006) 8086–8098.
[16] W.H. Miller, M.A. Seefeld, K.A. Newlander, I.N. Uzinskas, W.J. Burgess, D.A. Heerding, C.C.K. Yuan, M.S. Head, D.J. Payne, S.F. Rittenhouse, T.D. Moore, S.C. Pearson, V. Berry, W.E. DeWolf, B.J. Poloizzi, X. Qiu, C.A. Janson, Discovery of aminopyridine-based inhibitors of bacterial enoyl-ACP reductase (FabI), J. Med. Chem. 45 (2002) 3246–3256.
[17] N. Kaplan, M. Albert, D. Awrey, E. Bardouniotis, J. Berman, T. Clarke, M. Dorsey, B. Hafkin, J. Ramnauth, V. Romanov, M.B. Schmid, R. Thalakada, J. Yethon, H.W. Pauls, Mode of action, *in vitro* activity and *in vivo* efficacy of AFN-1252, a selective antistaphylococcal FabI inhibitor, Antimicrob. Agents Chemother. 56 (2012) 5865–5874.
[18] S. Escaich, L. Prouvensier, M. Saccomani, L. Durant, M. Oxoby, V. Gerusz, F. Moreau, V. Vongsothi, C. Maher, I. Morrisey, C. Soulama-Mouze, The

MUT056399 inhibitor of FabI is a new antistaphylococcal compound, Antimicrob. Agents Chemother. 55 (2011) 4692–4697.
[19] T. Bogdanovich, C. Clark, K. Kosowka-shick, B. Dewasse, P. McGhee, P.C. Applebaum, Antistaphylococcal activity of CG400549, a new experimental FabI inhibitor compared with that of other agents, Antimicrob. Agents Chemother. 51 (2007) 4191–4195.
[20] H. Schweiser, Triclosan: a widely used biocide and its link to antibiotics, FEMS Microbiol. Lett. 202 (2001) 1–7.
[21] M. Takhi, C. Murugan, M. Munikumar, K.M. Bhaskarreddy, G. Singh, K. Sreenivas, M. Sitaramkumar, N. Selvakumar, J. Das, S. Trehan, J. Iqbal, Synthesis and antibacterial activity of novel oxazolidinones bearing N-hydroxyacetamidine substituent, Bioorg. Med. Chem. Lett. 16 (2006) 2391–2395.
[22] M. Takhi, G. Singh, C. Murugan, N. Thaplyyal, S. Maitra, K.M. Bhaskarreddy, P.V.S. Amarnath, A. Mallik, T. Harisudan, R.K. Trivedi, K. Sreenivas, N. Selvakumar, J. Iqbal, Novel and potent oxazolidinones featuring 3-indolylglyoxamide, Bioorg. Med. Chem. Lett. 18 (2008) 5150–5155.
[23] PDB Reference 4JQC.
[24] While our work on azetidine ene-amide series was in progress, FAB pharma published a patent having close prior art,[25] where compounds **AEA1-3** and **AEA16** were disclosed.
[25] V. Gerusz, S. Escaich, M. Oxoby, A. Denis, Novel heterocyclic acrylamides and their use as pharmaceuticals, PCT Intl. Appl. (2011). WO 061214A1.
[26] H. Bregman, J.L. Buchanan, N. Chakka, E.F. Dimauro, B. Du, H.N. Nguyen, X.M. Zheng, Aryl carboxamide derivatives as sodium channel inhibitors for treatment of pain, PCT Intl. Appl. (2011). WO 103196.
[27] W.A. Slusarchyk, S.A. Bolton, K.S. Hartl, M.H. Huang, G. Jacobs, W. Meng, M.L. Ogletree, Z. Pi, W.A. Schumacher, S.M. Seiler, J.C. Sutton, U. Treuner, R. Zahler, G. Zhao, G. Bisacchi, Synthesis of potent and highly selective inhibitors of human tryptase, Bioorg. Med. Chem. Lett. 12 (2002) 3235–3238.
[28] M.A.J. Duncton, M.A. Estiarte, R.J. Johnson, M. Cox, D.J.R. O'Mahony, W.T. Edwards, M.G. Kelly, Preparation of heteroaryloxetanes and heteroarylazetidines by use of Minisci reaction, J. Org. Chem. 74 (2009) 6354–6357.
[29] M. Takhi, H. Subramanya, S.K. Panigrahi, M. Munikumar, K.C. Reddy, Substituted pyridine derivatives as FabI inhibitors, PCT Intl. Appl. (2013). WO 080222.
[30] J. Berman, P. Sampson, H.W. Pauls, J. Ramnauth, D. Manning, M.D. Surman, D. Xie, H.Y. Decornez, Heterocyclic compounds, methods of making them and their use in therapy, PCT Intl. Appl. (2004). WO 052890.
[31] J.M. Berman, M.D. Schmid, J.D. Medelin, N. Kaplan, Compositions Comprising Multiple Bioactive Agents, and Methods of Using the Same, US0142265A1 (2006).
[32] R. O'Shea, H.E. Moser, Physicochemical properties of antibacterial compounds: implications in drug discovery, J. Med. Chem. 51 (2008) 2871–2878.
[33] PDB Reference 4JX8.
[34] J. Schiebel, A. Chang, S. Shah, Y. Lu, L. Liu, P. Pan, M.W. Hirschbeck, M. Tareilus, S. Eltschkner, W. Yu, J.E. Cummings, S.E. Knudson, G.R. Bommineni, S.G. Walker, R.A. Slayden, C.A. Sotriffer, P.J. Tonge, C. Kisker, Rational design of broad spectrum antibacterial activity based on a clinically relevant enoyl-acyl carrier protein (ACP) reductase inhibitor, J. Biol. Chem. 289 (2014) 15987–16005.
[35] X. Qiu, C.A. Janson, R.I. Court, M.G. Smyth, D.J. Payne, S.S. Abdel-Meguid, Molecular basis for triclosan activity involves a flipping loop in the active site, Protein Sci. 8 (1999) 2529–2532.
[36] Y. Li, W. G Lai, A. Whitcher-Johnstone, C.A. Busacca, M.C. Eriksson, J.C. Lorenz, D.J. Tweedie, Metabolic switching of BILR 355 in the presence of ritonavir. I. Identifying an unexpected disproportionate human metabolite, Drug. Metab. Dispos. 40 (2012) 1122–1129.
[37] M.J. Stewart, S. Parikh, G. Xiao, P.J. Tonge, C. Kisker, Structural basis and mechanism of enoyl reductase inhibition by triclosan, J. Mol. Biol. 290 (1999) 859–865.
[38] Z. Otwinowski, W. Minor, Processing of X-ray diffraction data collected in oscillation mode, in: C.W. Carter Jr., R.M. Sweet (Eds.), Methods in Enzymology, Macromolecular Crystallography, Part A, vol. 276, Academic Press, New York, 1997, pp. 307–326.
[39] Collaborative Computational Project, Number 4, The CCP4 suite: programs for protein crystallography, Acta Crystallogr. D Biol. Crystallogr. 50 (1994) 760–763.
[40] A.A. Vagin, R.S. Steiner, A.A. Lebedev, L. Potterton, S. McNicholas, F. Long, G.N. Murshudov, REFMAC5 dictionary: organisation of prior chemical knowledge and guidelines for its use, Acta Crystallogr. D60 (2004) 2284–2295.
[41] P. Emsley, K. Cowtan, Coot: model-building tools for molecular graphics, Acta Crystallogr. D60 (2004) 2126–2132.
[42] W.L. DeLano, The PyMOL Molecular Graphics System, 2002 on World Wide Web, http://www.pymol.org.